Quantitative Mapping of Human Hair Graying and Reversal in Relation to Life Stress

Ayelet Rosenberg[1], Shannon Rausser[1], Junting Ren[2], Eugene Mosharov[3, 4], Gabriel Sturm[1], R Todd Ogden[2], Purvi Patel[5], Rajesh Kumar Soni[5], Clay Lacefield[4], Desmond J Tobin[6], Ralf Paus[7,8], Martin Picard[1,4,9,*]

[1] Department of Psychiatry, Division of Behavioral Medicine, Columbia University Medical Center, New York, NY, USA

[2] Department of Biostatistics, Mailman School of Public Health, Columbia University Medical Center, New York, NY, USA

[3] Department of Psychiatry, Division of Molecular Therapeutics, Columbia University Medical Center, New York, NY, USA

[4] New York State Psychiatric Institute, New York, NY USA

[5] Proteomics and Macromolecular Crystallography Shared Resource, Columbia University Irving Medical Center, New York, NY, USA

[6] UCD Charles Institute of Dermatology & UCD Conway Institute, School of Medicine, University College Dublin, Dublin, Ireland

[7] Dr. Phillip Frost Department of Dermatology & Cutaneous Surgery, University of Miami Miller School of Medicine, Miami, FL, USA

[8] Centre for Dermatology Research, University of Manchester, Manchester, UK

[9] Department of Neurology, H. Houston Merritt Center, Columbia Translational Neuroscience Initiative, Columbia University Medical Center, New York, NY, USA

Summary

Hair graying is a universal hallmark of chronological and biological aging, but its mechanisms are insufficiently understood and its potential reversibility in humans has not been quantitatively examined. Moreover, while psychological stress accelerates human biological aging and triggers hair graying in animals, no prior study has longitudinally examined the stress-to-hair graying connection in humans. Here we develop a novel approach to quantitatively profile natural graying events and their associated proteomic signatures along individual human hair shafts, resulting in a quantifiable physical timescale of hair pigmentation patterns (HPPs). Using this approach, we quantify rare events of white/gray hairs that naturally regain pigmentation within days to weeks, in 14 individuals across sex, ethnicities, ages, and body regions, thereby quantitatively defining the reversibility of graying across hairs in healthy, unmedicated individuals. Proteomic analysis of matched dark (i.e. pigmented) and white hairs replicated across two independent experiments show that graying is marked by the upregulation of proteins related to energy metabolism, mitochondria, and antioxidant defenses. Combining hair pigmentation profiling and proteomics at the single hair level, we also report hair graying and its reversal occurring in parallel with behavioral and psychological stressors. A computational simulation of life-long and stress-induced hair graying suggests a threshold-based mechanism for the episodic instability of HF pigmentation and the temporary reversibility of graying. Our results show how quantitatively mapping HPPs in humans can provide an opportunity to examine the modifiability of biological aging in relation to life exposures.

Keywords: human aging; hair graying; reversal; psychological stress; mitochondria.

Hair graying is a ubiquitous, visible, and early feature of human biological aging[1]. In aging mammalian tissues, senescent cells appear stochastically beginning early in life[2,3]. Similarly, individual hair follicles (HFs) on the scalp and other body regions undergo depigmentation in a stochastic, age-related manner[4]. Phenotypically, the age-related instability and depigmentation of the HF therefore parallels the increased episodic molecular instability[5] and cell-to-cell heterogeneity that characterizes biological aging[6-8]. In mice, cells expressing canonical senescent signatures (e.g., $P16^{INK4a}$) begin to appear in multiple organs as early as a few weeks after birth[3,9], documenting age-related cellular transitions appearing early in life. Sensitive detection methods in tissues with unambiguous age-related phenotypes, such as hair shaft depigmentation or graying, could similarly reveal early age-related phenotypes and their modifiability in humans.

The time of onset of hair graying varies between individuals, as well as between individual hair follicles, based on genetic and other biobehavioral factors[10]. But most people experience depigmentation of a progressively large number of hair shafts (HSs) from their third decade onward, known as achromotrichia or canities[11]. The color in pigmented HSs is provided by melanin granules, a mature form of melanosomes continuously supplied to the trichocytes of the growing hair shaft by melanocytes of the hair follicle pigmentary unit (HFPU)[1]. Age-related graying is thought to involve melanocyte stem cell (MSC) exhaustion[12], neuroendocrine alterations[13], and other factors, with oxidative damage to the HFPU likely being the dominant, initial driver[13-15]. While loss of pigmentation is the most visible change among graying hairs, depigmented hairs also differ in other ways from their pigmented counterparts[16], including in their growth rates[17], HF cycle and other biophysical properties[18]. Hair growth is an energetically demanding process[19] relying on aerobic metabolism in the HF[20]. Melanosome maturation also involves the central organelle of energy metabolism, mitochondria[21,22]. Moreover, mitochondria likely contribute to oxidative stress within the HF[23], providing converging evidence that white hairs may exhibit specific alterations in mitochondrial energy metabolism.

Although hair graying is generally considered a progressive and irreversible age-related process, with the exclusion of alopecia areata[24], various cases of drug- and mineral deficiency-induced depigmentation or repigmentation of hair have been reported[25-31] reflecting the influence of environmental inputs into HFPU function[32]. While spontaneous repigmentation can be pharmacologically-induced, its natural occurrence in unmedicated individuals is rare and has only been reported in a few single-patient case studies[33-37]. A proposed mechanism for such repigmentation events involve the activation and differentiation of a subpopulation of immature

melanocytes located in a reservoir outside of the hair follicle bulb in the upper outer root sheath[18]. However, the reversal of hair graying has not yet been quantitatively examined in a cohort of healthy adults, in parallel with molecular factors and psychosocial exposures.

The influence of psychological stress on hair pigmentation is a debated but poorly documented aspect of hair graying. In humans, psychological stress accelerates biological aging as measured by telomere length[38,39]. In mice, psychological stress and the stress mediator norepinephrine acutely causes depigmentation[40], but in mice graying is an irreversible phenomenon driven by a depletion of melanocyte stem cells[15]. In humans, where HF biology differs significantly from rodents[37], stress-induced graying and its reversal remain insufficiently understood. The paucity of quantitative data in humans is mostly due to the lack of sensitive methods to precisely correlate stressful psychobiological processes with hair pigmentation and graying events at the single-follicle level.

Here we describe a digitization approach to map hair pigmentation patterns (HPPs) in single hairs undergoing graying and reversal transitions, examine proteomic features of depigmented white hairs, and illustrate the utility of the HPP approach to interrogate the association of life stress and hair graying in humans. Because previous literature suggests that rare pigmentation events are more likely to occur in the early stages of canities[18], the current study focuses primarily on pigmentation events in young to middle-aged participants. Finally, we develop a computational model of hair graying to explore the potential mechanistic basis for stress-induced graying and reversibility on the human scalp hair population, which could potentially serve as a resource for the *in silico* modelling of macroscopic aging events in human organs/tissues.

Results

Mapping hair pigmentation patterns (HPPs)

To overcome the lack of methodology to map pigmentary states and age-related graying transitions, we developed an approach to digitize HPPs at high resolution across the length of single human HSs. Combined with known hair growth rates on the scalp (~1.0-1.3 cm per month[41]), this approach provides a quantifiable, personalized live bioarchive with the necessary spatio-temporal resolution to map individualized HPPs and graying events along single hairs, and to link HPPs to specific moments in time with unprecedented accuracy. Using this methodology, similar to dendrochronology where tree rings represent elapsed years[42], hair length reflects time, and the HS length is viewed as a physical time scale whose proximal region

has been most recently produced by the HF, and where the distal hair tip represents weeks to years in the past, depending on the HS length.

To examine HPPs in human hairs, we plucked, imaged, digitized, and analyzed hairs (n=397) from 14 healthy donors (**Figure 1A**) (see Methods for details). Three main pigmentation patterns initially emerged from this analysis: i) Hairs with constant high optical density (*Dark*), ii) Hairs with constant low optical density (*White*); iii) Initially dark hairs that undergo a sharp graying transition from dark to white over the course of a single growing anagen phase of the hair follicle growth cycle (*Transition*) (**Figure 1B-C**). Dark-to-white transitions demonstrate the existence of rapid depigmentation events within a single anagen hair cycle[43,44]. We confirmed that compared to dark hairs still harboring their "young" pigmentary state, the HFPU of "aged" white HFs from either African American or Caucasian individuals are practically devoid of pigment (**Figure 1D**), which is consistent with the finding of previous studies[45]. Whereas dark hairs contain melanin granules dispersed throughout the hair cortex when observed by electron microscopy, white hairs from the same individuals show a near complete (>98%) absence of melanin, with the few retained melanin granules, when present, being smaller, less dense, and at times vacuolated, a potential response to oxidative stress[46] (**Figure 1E-I**, see **Supplemental Figure S1** for high-resolution images of mature melanosomes). The digitization of HPPs thus reflects the presence of melanosomes within the HS, and rapid graying events are marked by the loss of melanosomes.

Proteomic alterations in white hairs

To gain molecular insight into the graying process, we performed a comprehensive proteomic analysis comparing dark and white HS. Recent work suggests that depigmentation is associated with the upregulation of lipid synthesis enzymes in the HS[47]. Moreover, in depigmented hairs, the abnormal diameter/caliber of the hair fiber, growth rate, presence/absence of HS medulla as well as the (dis)continuity and diameter of the medulla along the hair length[48] imply multiple potential proteomic alterations associated with depigmentation. In addition, melanogenesis involves high levels of reactive oxygen species, but dark HFs are equipped with multiple antioxidant mechanisms (e.g.,[46]). Thus, the proteomic features of HSs may provide interpretable information about molecular changes associated HF graying.

Protein extraction and LC-MS/MS methods optimized from a previous protocol[49] were used to process the unusually resistant proteinaceous matrix of the hair shaft and to handle the

119 overly abundant keratin proteins over other potential proteins of interest (see Methods for
120 details). Two independent experiments were performed. *Experiment 1*: matched dark and white
121 hairs collected at the same time from two closely age- and diet-matched individuals (1 female
122 and 1 male, both 35 years old, each dark and white HS measured twice, total n=8); and
123 *Experiment 2 (validation):* n=17 hair segments from 7 different individuals (4 females and 3
124 males).

125 In the first experiment, we were able to extract and quantify 323 proteins (>75% of
126 samples) from single 2 cm-long HS segments. Compared to dark HS collected at the same time
127 from the same individuals, white hairs contained several differentially enriched (upregulated) or
128 depleted (downregulated) proteins (**Figure 1J-K** see **Supplemental Table S1** for complete list)
129 on which we performed GO (Gene Ontology) and KEGG (Kyoto Encyclopedia of Genes and
130 Genomes) enrichment analysis and explored their protein-protein interaction networks
131 (**Supplemental Figure S2**). The protein networks for both downregulated (<0.8-fold, n=23) and
132 upregulated (>1.5-fold, n=67) proteins contain significantly more interactions than expected by
133 chance (P<0.00001, observed vs expected protein-protein interactions). Thus, coherent groups
134 of functionally related proteins are differentially expressed in white hairs, from which two main
135 patterns emerged.

136 The first main pattern relates to protein biosynthesis and energy metabolism. A large
137 fraction (34.3%) of upregulated proteins in white hairs was related to ribosome function, protein
138 processing, and associated cytoskeletal proteins. Upregulation of the machinery responsible for
139 protein synthesis and amino acid metabolism included the ribosomal protein RPS15A, which is
140 known to localize to mitochondria. Of all upregulated proteins in white hairs, 26.8% were known
141 mitochondrial proteins (MitoCarta2.0 and others)[50]. These proteins are involved in various
142 aspects of energy metabolism, including substrate transport (carnitine palmitoyltransferase 1A,
143 CPT1A; malonate dehydrogenase 1, MDH1), respiratory chain function (Complex III subunit 1,
144 UQCRC1), and catecholamine homeostasis (Catechol-O-Methyltransferase, COMT). White
145 hairs also contained more proteins involved in glucose (glucose 6-phosphate dehydrogenase,
146 G6PD; phosphoglycerate kinase 1, PGK1) and lipid metabolism located in either the
147 mitochondria or cytoplasm (fatty acid synthase, FASN; acyl-CoA thioesterase 7, ACOT7;
148 mitochondrial trifunctional enzyme subunit beta, HADHB) or in peroxisomes (acyl-CoA
149 acyltransferase 1, ACAA1). The metabolic remodeling in white hairs is consistent with the
150 established role of mitochondria and metabolic regulation of hair growth and maintenance in
151 animal models[19,51-53], and possibly consistent with hair anomalies reported in human patients

with mitochondrial disease[54]. The upregulation of energy metabolism may subserve the likely increased energy demands in depigmented hairs. However, our data and those of others[47] implicate the upregulation of specific mitochondrial proteins involved, not necessarily in global energy metabolism, but in specific metabolic activities such as amino acid and lipid biosynthesis.

A second less robust pattern relates more directly to melanosome biology. In line with the lysosomal origin of melanosomes that are largely absent in depigmented HS[44], several lysosomal proteins (PLD3, CTSD, HEXB, and LAMP1) were downregulated in white hairs, consistent with previous literature[47]. White hair shafts also showed a depletion of six main keratins (see **Figure S2**), likely because graying can affect the nature of keratinocytes proliferation[18], of proteins associated with exocytosis, such as ITIH4 and APOH (potentially involved in the secretion of melanosomes from melanocytes to keratinocytes), as well as proteins associated with mitochondrial calcium transmembrane transport. Interestingly, calcium exchange between mitochondria and the melanosome is required for melanin pigment production in melanocytes[21], and calcium signaling promotes melanin transfer between melanosomes and keratinocytes[55].

Finally, canities-affected white HFs also showed upregulation of antioxidant proteins, specifically those localized to mitochondria and cytoplasm (superoxide dismutase 1, SOD1; peroxiredoxin 2, PRDX2), in line with the role of oxidative stress in HS depigmentation[14,56]. Alterations among these individual metabolic and mitochondrial enzymes were further reflected in KEGG pathways functional enrichment analyses indicating a significant enrichment of metabolic pathways including carbon metabolism and fatty acid synthesis, amino acids, and oxidative phosphorylation (see below).

Validation of graying-associated proteomic signatures

To independently validate these results, we extended this analysis to white and dark HS from 6 individuals (3 males, 3 females, range: 24-39 years) analyzed on a separate proteomic platform and in a different laboratory. In this experiment, a total of 192 proteins (≥3 samples) were quantified from 1cm-long HS segments. This dataset showed a similar trend as the first analysis towards a preferential overexpression of proteins with graying (55% upregulated vs 29% downregulated in white HS) (**Figure 1L-M,** see **Supplemental Table S2** for a complete list). The most highly upregulated proteins included mitochondrial components such as the voltage-dependent anion channel 1 (VDAC1), a subunit of ATP synthase (ATP5A1), and a

regulator of mitochondrial respiratory chain assembly (Prohibitin-2, PHB2). Again, the antioxidant enzyme SOD1 was enriched in white relative to dark HSs.

To examine the possibility that these relative upregulations are driven by a global downregulation of highly abundant housekeeping proteins, we analyzed the intensity-based absolute quantification (iBAQ) data for each sample. This confirmed that the housekeeping proteins, including keratins and keratin-associated proteins, were not downregulated in white hairs, but generally unchanged or slightly upregulated. Moreover, as a whole, upregulated proteins formed a coherent protein-protein interactions cluster ($p<0.00001$) and pathway analysis showed a significant enrichment of carbon metabolism, glycolysis/glucogenesis, pyruvate metabolism, and amino acid synthesis pathways in white relative to dark HS (**Supplemental Figure S3, Figure 4E**). On the other hand, proteins downregulated in white HSs were related to cholesterol metabolism, complement-coagulation cascades, and secretory processes shared with immune/inflammatory pathways (**Figure 4E**). The downregulation of secretory pathways is again consistent with reduced transfer of pigmented melanosomes from the melanocytes to the keratinocytes.

To verify the robustness of these findings using an alternative analytical approach, we built a simple partial least square discriminant analysis (PLS-DA) multivariate model, which provided adequate separation of white vs dark HS (**Supplemental Figure S4**). Simple interrogation of this model to extract the features (i.e., proteins) that maximally contribute to group separation yielded a set of proteins enriched for estrogen signaling pathways, complement and coagulation cascades, as well as metabolic pathways including NAD^+/NADH, cholesterol, pyruvate, and carbon metabolism, similar to results above. Interestingly, we also identified 13 proteins that were undetectable in any of the dark HS (either not expressed, or below the detection limit), but consistently present in white HS (**Supplemental Table S3**). These proteins are either newly induced or experience a substantial upregulation with graying (fold change tending towards infinity). A separate functional enrichment analysis for these induced proteins also showed significant enrichment for the same aging-related metabolic pathways as for the upregulated protein list: glycolysis/glucogenesis, carbon, pyruvate, and cysteine and methionine metabolism (all $P<0.001$).

These converging proteomics data, which are consistent with previous findings[47], support a multifactorial process directly implicating metabolic changes in human hair graying[13]. Moreover, given that metabolic pathways are rapidly and extensively remodeled by environmental and neuroendocrine factors – i.e., they naturally exhibit plasticity – these data

build upon previous proteomic evidence to show that human hair graying could be, at least temporarily, reversible

Human hair graying is, at least temporarily, reversible

Our analysis of HPPs in healthy unmedicated individuals revealed several occasions whereby white hairs naturally revert to their former dark pigmented state. This phenomenon was previously reported only in a handful of case reports, with only a single two-colored HS in each case[37]. Here we document the reversal of graying along the same HS in both female and male individuals, ranging from a prepubescent child to adults (age range 9 to 39 years), and across individuals of different ethnic backgrounds (1 Hispanic, 12 Caucasian, 1 Asian). This phenomenon was observed across frontal, temporal, and parietal regions of the scalp (**Figure 2A**), as well as across other corporeal regions, including pubic (**Figure 2B**) and beard hairs (**Figure 2C**). The existence of white HS undergoing repigmentation across ages, sexes, ethnicity, and corporeal regions documents the reversibility of hair graying as a general phenomenon not limited to scalp hairs. Nevertheless, we note that this phenomenon is limited to rare, isolated hair follicles. As their occurrence will probably go unnoticed in most cases, it is difficult to assess the true incidence of these events. Still, only a limited number of case studies reporting natural reversibility of graying appear in the literature, and we were only able to identify 14 participants over an active recruitment period of 2.5 years, indicative of the rarity of this phenomenon.

Moreover, more complex HPPs with double transitions and reversions in the same HS were observed in both directions: HS undergoing graying followed by rapid reversal (**Figure 2D**), and repigmentation rapidly followed by graying (**Figure 2E**). Importantly, both patterns must have occurred over the course of a single anagen (growth) phase in the hair growth cycle, implicating cellular mechanisms within the HFPU. Greatly extending previous case studies of these rare hair repigmentation events, the current study provides the first quantitative account of the natural and transitory reversibility of hair graying in humans.

We understand the emergence of a reverted HS – that is, a HS with a white distal segment but with a dark proximal end – as necessarily having undergone repigmentation to its original pigmented state following a period of time as a depigmented “old” white hair (**Figure 2F**). In double transition HS with three segments, repigmentation must take place within weeks to months after graying has occurred, producing three distinct segments present on the same hair strand (**Figure 2G**). Microscopic imaging along the length of a single HS undergoing a

double transition (graying followed by rapid reversal) can be visualized in **Video S1**, illustrating the dynamic loss and return of pigmented melanosomes within the same HS.

Our hair digitization approach also provides the first estimates of the rates of change in pigmentation for HS covering a broad range of initial colors and darkness (**Figure 2H**). Across individuals, assuming a scalp hair growth rate of 1 cm/month[41], the rates of depigmentation in graying hairs ranged widely from 0.3 to 23.5 units of hair optical density (scale of 0-255 units) per day, corresponding to between 0.2% and 14.4% loss of hair color per day (**Figure 2I**). The rate at which HS regain pigmentation during reversal was 0.1 to 42.5 units per day, which is similar (~30% faster on average) to the rate of graying (Cohen's d = 0.15, p = 0.59) (**Figure 2J**). Given these rates, the fastest measured transitioning hairs gray and undergo full reversal in ~3-7 days (median: ~3 months). Thus, rather than drifting back towards the original color, repigmentation of white human HS occurs within the same time frame and at least as rapidly as the process of graying itself.

The spectrum of graying transitions and reversals patterns observed in our cohort, including measured rates of repigmentation along individual hairs, is shown in **Supplemental Figure S5**. These results establish the wide range of naturally-occurring rates of pigmentary changes in single hairs, which vary by up to an order of magnitude from hair to hair. These data also suggest that reversal/repigmentation may reflect the action of as yet unknown local or systemic factors acting on the HFPU within a time frame of days to weeks.

Correlated behavior of multiple scalp hairs

We then asked whether the reversal of graying is governed by a process that is unique to each human scalp HF or if it is likely coordinated by systemic factors that simultaneously affect multiple HFs. Participants' scalps were visually inspected to identify two-colored hairs, including both graying transitions and reversal. In our combined cohort, three individuals had multiple two-colored hairs collected at either one or two collection times within a one-month interval. In each case, the multiple two-colored hairs originated from independent HFs separated by at least several centimeters (e.g., left vs right temporal, or frontal vs temporal). If the hairs are independent from each other, the null hypothesis is that different HSs will exhibit either graying or reversal changes and will have independent HPPs. If multiple HSs were coordinated by some systemic factor, then we expect HPPs to exhibit similarities.

In a first 35-year-old female participant with dark brown hair, 3 two-colored hairs were identified at a single instance of collection. Notably, all three hairs exhibited dark-to-white

graying. Moreover, when the HPPs of the 3 hairs were quantified and plotted, the HPPs followed strikingly similar graying trajectories (r=0.76-0.82) marked by a similar onset of graying, similar HPP intermittent fluctuations (note the rise ~10 cm), and a similar time point where all hairs become fully depigmented (~15 cm) (**Figure 3A**). A permutation test on the similarity of the color trajectories yielded p=0.032, suggesting possible synchrony between different HSs. If our simulation considers only hairs that transition in one direction (from dark to white) this gives p=0.086 (see *Methods* for details).

In a 37-year-old female participant with brown hair, two transition hairs were identified. The HPPs for both hairs revealed strikingly similar trajectories (r=0.80), in this case undergoing spontaneous reversal in a near-synchronous manner upon alignment ($p<0.001$ when considering hairs transitioning in either direction, and similarly, $p<0.001$ considering only hairs transitioning from white to dark, **Figure 3B**). Thus, these findings extend previous reports in single isolated hairs by providing quantitative accounts of coordinated HS (re)pigmentation across multiple hairs.

Candidate humoral hair pigmentation modulators that could create synchrony in graying or repigmenting hairs include neuropeptides, redox balance, and steroid or catecholamine hormones[32,40,57,58] that can directly regulate the human HFPU[13], impact intrafollicular clock activity[57], or regulate the expression of other melanotropic neurohormones in the human HFPU such as α-MSH, ß-endorphin, and TRH[59]. These factors must act in parallel with genetic factors that influence inter-individual differences in aging trajectories.

Hair graying and reversal are linked to psychosocial stress levels

In light of these results, we next applied our HPP method to examine the possibility that psychological stress is associated with hair graying/reversal in humans. Anecdotal case reports suggest that psychological stress and other behavioral factors accelerate the hair graying process[60], a notion recently supported by studies in mice demonstrating that adrenergic stimulation by norepinephrine signaling leads to melanocyte stem cell depletion in mice[40]. However, contrary to mice where this process appears to be irreversible at the single hair follicle level, our data demonstrates that human hair graying is, at least under some circumstances, reversible. This dichotomy highlights a fundamental difference between rodent and human HF biology, calling for a quantitative examination of this process in humans.

As evidence that environmental or behavioral factors influence human hair graying, epidemiological data suggests that smoking and greater perceived life stress, among other

314 factors, are associated with premature graying[10]. Chronic psychosocial stress also precipitates
315 telomere shortening, DNA methylation-based epigenetic age, as well as other biological age
316 indicators in humans[39,61], demonstrating that psychological factors can measurably influence
317 human aging biology. In relation to mitochondrial recalibrations, psychosocial factors and
318 induced stress can also influence mitochondrial energetics within days in humans[62] and
319 animals[63]. To generate proof-of-concept evidence and test the hypothesis that psychosocial or
320 behavioral factors may influence graying at the single-HF level, we leveraged the fact that HPPs
321 reflect longitudinal records of growth over time – similar to tree rings – which can be aligned with
322 assessments of life stress exposures over the past year. By converting units of hair length into
323 time, perceived stress levels can be quantitatively mapped onto HPPs in both graying and
324 transitional hairs.

325 A systematic survey of two-colored hairs on the scalp of a 35-year-old Caucasian male
326 with auburn hair color over a two-day period yielded five two-colored HS from the frontal and
327 temporal scalp regions. Again, two-colored hairs could either exhibit depigmentation or reversal.
328 Unexpectedly, all HS exhibited reversal. HPP analysis further showed that all HS underwent
329 reversal of graying around the same time period. We therefore hypothesized that the onset of
330 the reversal would coincide with a decrease in perceived life stress. A retrospective assessment
331 of psychosocial stress levels using a time-anchored visual analog scale (participants rate and
332 link specific life events with start and end dates, see *Methods* and **Supplemental Figure S6** for
333 details) was then compared to the HPPs. The reversal of graying for all hairs coincided closely
334 with the decline in stress and a 1-month period of lowest stress over the past year (0 on a scale
335 of 0-10) following a two-week vacation (**Figure 3C**).

336 We were also able to examine a two-colored hair characterized by an unusual pattern of
337 complete HS graying followed by rapid and complete reversal (same as in Figure 2B) plucked
338 from the scalp of a 30-year-old Asian female participant with black hair. HPP analysis of this HS
339 showed a white segment representing approximately 2 cm. We therefore hypothesized that this
340 reversible graying event would coincide with a temporary increase in life stress over the
341 corresponding period. Strikingly, the quantitative life stress assessment over the last year
342 revealed a specific 2-month period associated with an objective life stressor (marital conflict and
343 separation, concluded with relocation) where the participant rated her perceived stress as the
344 highest (9-10 out of 10) over the past year. The increase in stress corresponded in time with the
345 complete but reversible hair graying (**Figure 3D**). This association was highly significant
346 ($p=0.007$) based on our permutation test. Given the low statistical probability that these events

are related by chance, life stress is the likely preceding cause of these HS graying and reversal dynamics. These data demonstrate how the HPP-stress mapping approach makes it possible to examine the coordinated behavior of graying and reversal dynamics with psychosocial factors, raising the possibility that systemic biobehavioral factors may influence multiple HFs simultaneously and regulate HPPs among sensitive hairs.

Single-hair longitudinal proteomic signature

To assess whether rapid graying and reversal events among a single hair are molecularly similar or distinct to those described in the two proteomics experiments above, we dissected 6 segments (2 dark, 2 white, 2 reverted) of the single HS in Figure 3D and quantified their proteomes as part of Experiment 2. This produced a longitudinal, single-hair, proteomic signature (**Figure 3E**) containing 301 proteins quantified in ≥2 of the 6 segments. To examine how the proteome as a whole is altered through the graying and reversal transitions associated with psychosocial stress levels, we generated a PLS-DA model with all 6 segments. Both dark segments clustered together, with similar values on both first and second principal components. The white and reverted segments clustered in separate topological spaces (**Figure 3F**). Graying was associated with a positive shift largely along the first component (Component 1), whereas reversal was associated with a negative shift on the second component (Component 2) and a more modest negative shift in Component 1. We therefore extracted loading weights of each protein on Components 1 and 2 (reflecting each protein's contribution to group separation) and used the top proteins (n=20 highest negative and 20 most positive loadings, total n=40 per component) to interrogate KEGG and GO databases.

The model's Component 1 (associated with graying) contained proteins that were either i) not expressed in the dark HS but induced selectively in the white HS segment, or ii) highly abundant in dark segments but strongly downregulated in white and reverted segments (**Figure 3H**, *top* and *bottom*, respectively). In gene set enrichment analysis of Component 1 (graying), the top three functional categories were carbon metabolism, glycolysis/gluconeogenesis, and Kreb's cycle (**Figure 4E**). Component 2 (reversal)-associated proteins exhibited distinct trajectories either peaking in the first white segment or upon reversal (**Figure 3I**) and mapped to pathways related to the complement activation cascade, infectious processes, and Parkinson's and Huntington's disease (**Figure 4E**). In contrast, a null set of hair proteins not contributing to either components exhibited enrichment for extracellular exosomes and cell-cell adhesion that reflect hair shaft biology (Supplemental Figure S7), therefore illustrating the specificity of our findings related to graying and reversal. These data indicate that the reversal of graying at the

single-hair level is not associated with a complete reversal in the molecular composition of the HS. Rather, some of the proteomic changes in hair graying are enduring despite successful repigmentation.

Conserved proteomic signatures of hair graying

To systematically examine the overlap among the different proteomic datasets and to derive functional insight into the hair graying process in humans, we then integrated results from the three datasets described above. White HS show consistently more upregulated than downregulated proteins across datasets (2.91-fold in Experiment 1, 1.89-fold in Experiment 2) (**Figure 4A**). This preferential upregulation suggests that the depigmentation process likely involves active metabolic remodeling rather than a passive loss of some pigmentation-related factor. The overlap in the specific proteins identified across dark-white comparisons and among the 6-segments hair is illustrated in **Figure 4B**.

Five proteins were consistently upregulated between experiments 1 and 2. These include three well-defined resident mitochondrial proteins involved in lipid metabolism: CPT1A, which imports fatty acids into mitochondria[64]; ACOT7, which hydrolyzes long-chain fatty acyl-CoA esters in the mitochondrial matrix and cytoplasm[65]; and SOD1, which dismutates superoxide anion into hydrogen peroxide (H_2O_2) in the mitochondrial intermembrane space[66]. The other two proteins include the actin-depolymerizing protein cofilin-1 (CFL1) and the core glycolysis enzyme phosphoglycerate kinase 1 (PGK1) (**Figure 4C**). Interestingly, CFL1 promotes mitochondrial apoptotic signaling via cytochrome c release[67] and regulates mitochondrial morphology via its effect on actin polymerization-dependent mitochondrial fission[68]. And although PGK1 is a cytoplasmic kinase, it was recently demonstrated to translocate inside mitochondria where it phosphorylates and inhibits pyruvate dehydrogenase and Krebs cycle activity[69]. Thus, all five proteins validated across both experiments are linked to mitochondrial energy metabolism, implicating mitochondrial remodeling as a feature of hair graying. Interestingly, all five proteins have also been linked to the biology of melanocytes[70-74], the source of pigment in the HFPU. The downregulated proteins were keratins, with small effect sizes, and not particularly robust. Analysis of the intensity based on absolute quantification (iBAQ) data confirmed the upregulation of these five mitochondrial proteins, and the absence of substantial changes in the keratins. Together, these data suggest that HS proteome profiling may provide a retrospective access to some aspect of melanocyte metabolism, which opens new possibilities to study HF aging biology.

Since the observed proteomic signatures are related to specific metabolic pathways rather than the typical high-abundance mitochondrial housekeeping proteins, we reasoned that the upregulation of these mitochondrial components unlikely reflects a bulk increase in total mitochondrial content. To investigate this point using an independent method, we quantified mitochondrial DNA (mtDNA) abundance in human HS by real-time qPCR. Both white and dark HSs contain similarly high levels of mtDNA (**Figure 4D**). The same was true in the follicles of the same hairs (**Supplemental Figure S8**). The similar mtDNA levels between dark and white hairs increases the likelihood that the reported proteomic changes reflect the induction of specific metabolic pathways associated with hair graying rather than bulk increase in mitochondrial mass.

Finally, to identify a general proteomic signature of graying hair, we compiled the enrichment scores for KEGG pathways across all datasets (**Figure 4E**). Consistent with the function of the individual proteins identified in both group comparisons (Experiments 1 and 2) and the multi-segment double-transition hair, white HS showed consistent upregulation of carbon metabolism and amino acid biosynthesis, glycolysis/gluconeogenesis, and general metabolic pathways relevant to aging biology[75]. Comparatively fewer pathways were consistently represented for downregulated proteins across independent experiments. In relation to hair biology, our data adds to previous efforts[47] and provides a quantitative map of the co-expression among keratin and non-keratin HS proteins across dark and white hairs (**Figure 4F**). Computing the cross-correlations for each protein pair revealed four main clusters among the HS proteome. As expected for hair, keratins were well-represented and constituted the main GO biological processes category for 3 of the 4 clusters. The top KEGG categories included glycolysis and estrogen signaling pathways, which also showed strong co-expression with each other, highlighting potential interaction among endocrino-metabolic processes in relation to human hair pigmentation. In general, the identification of several non-keratin metabolism-related proteins in the HS opens new opportunities to investigate graying pathobiology and to non-invasively access past molecular and metabolic changes that have occurred in the aging HFPU of the dynamically growing hair.

In silico modeling of hair graying and its temporary reversal

Finally, to narrow the range of plausible mechanisms for the observed age-related graying and reversal events, we developed a simulation model of HPPs. Graying dynamics of an individual's hair population (~100,000 hairs) across the average 80-year lifespan cannot practically be measured. In the absence of such data, we propose here a mathematical model

to simulate hair graying trajectories across the human lifespan (**Figure 5A**, available online, see *Methods* for details) as has been attempted previously for hair growth cycles[76]. As basic tenets for this model, it is established that *i)* the onset of human hair graying is not yet underway and rarely begins in childhood, *ii)* graying routinely starts between 20-50 years of age, *iii)* graying is progressive in nature (the total number and percentage of gray hairs increases over time), and *iv)* the proportion of white hairs reaches high levels in old age, although some hairs can retain pigmentation until death, particularly among certain body regions[15]. Additionally, our findings demonstrate that *v)* age-related graying is naturally reversible in isolated hair follicles, at least temporarily and in individual HS, and may be acutely triggered by stressful life experiences, the removal of which can trigger reversal.

Aiming for the simplest model that accounts for these known features of hair graying dynamics, we found a satisfactory model with three components (**Figure 5B**): 1) an "*aging factor*" that progressively accumulates within each hair follicle, based on the fact that biological aging is more accurately modeled with the accumulation of damage, rather than a decline in stem cells or other reserves[77]; 2) a biological *threshold*, beyond which hairs undergo depigmentation (i.e., graying), characterizing the transition between the dark and white states in the same HS; and 3) a "*stress factor*" that acutely but reversibly increases the aging factor during a stressful event. For modeling purposes, the accumulation of the aging factor is equivalent to the inverse of the decrease in a youth factor (e.g., loss of telomere length with age). Based on the mosaic nature of scalp HFs and our data indicating that not all hairs are in perfect synchrony, the proposed model for an entire population of hairs must also allow a variety of aging rates, as well as differential sensitivity to stress among individual hairs.

We find that the model's predicted hair population behavior (% of white HSs on a person's head over time) across the lifespan is consistent with expected normal human hair graying dynamics (**Figure 5C**). White hairs are largely absent until the onset of graying past 20 years of age then accumulate before finally reaching a plateau around 70-90% of white hairs, near 100 years. Thus, this model recapitulates the expected between-hair heterogeneity of graying within an individual, producing the common admixture of white and pigmented hairs or "salt & pepper" phenotype in middle-age. However, some individuals also develop hairs with intermediate pigmentation states (i.e., silver/steel color), which our model does not reproduce. This represents a limitation to be addressed in future research.

We note that there are natural inter-individual differences in the rate of graying: some individuals begin graying early (onset in early 20's); some begin late (onset in 50's). A higher

rate of accumulation of the aging factor (higher slope for each hair) or a lower threshold naturally accounts for earlier onset of graying. In addition, our model reveals that within a person, greater hair-to-hair heterogeneity in the rate of aging between HFs, modeled as the standard deviation of slope across hairs, also influences the onset of graying. Greater heterogeneity between HFs allows for earlier onset of graying, whereas decreasing hair-to-hair variation (i.e., lower heterogeneity) is associated with a "youthful" later onset of graying (**Figure 5D**). Interestingly, this unpredicted result aligns with the notion that increased cell-to-cell heterogeneity is a conserved feature of aging[6-8] and that biological heterogeneity can predict all-cause mortality in humans[78].

Modeling stressors produce hair graying and temporary reversal

Using parameter values that yield the average onset and rate of graying, we then simulated the influence of acute psychosocial stressors, either early in life before the onset of graying, or later once gray HSs have begun to accumulate. Similar to our data, the model also predicts transitory, or temporary reversible events of graying (see Figure 3D). Transitory graying events do not affect all hairs, only those that are close to the threshold at the time of stress exposure undergo graying. Hairs whose cumulative aging factors are substantially lower than threshold do not show stress-induced graying (a 5-year-old is unlikely to get gray hairs from stress, but a 30-year-old can) (**Figure 5E-F**). Similarly, gray hairs far above threshold are not affected by periods of psychosocial stress. Thus, our model accounts for both the overall hair graying dynamics across the lifespan, and how a stressor (or its removal) may precipitate (or cause reversal of) graying in hairs whose aging factor is close to the graying threshold.

We speculate that this simulation opens an attractive possibility whereby HPP data from individuals could be used in models to formulate predictions about future graying trajectories, and to use HPPs and hair population graying behavior to track the effectiveness of behavioral and/or therapeutic interventions aimed at modifying human aging. Extending our high-resolution quantitative digitization approach to hundreds of randomly sampled dark non-transitioning hairs from different scalp regions in the same individuals, we also show that fully dark (i.e., non-graying) HSs exhibit mostly unique HPPs, but that hairs among the same scalp regions may exhibit more similar HPPs than hairs sampled from different regions (**Figure S9**)[79]. This may in part be influenced by the migration of stem cells during embryogenesis to different parts of the scalp, or by other unknown factors. This preliminary extension of the HPP methodology provides a foundation for future studies. Moreover, the regional segregation of HPPs may reflect well-recognized regional differences in the rate of HS formation[80]. Thus, future models may also

be able to leverage information contained within HPPs from non-graying hairs and make specific inference from hairs collected across scalp regions. Similar to how decoding temporal patterns of electroencephalography (EEG) provides information about the state of the brain, our data make it imaginable that decoding HPP analysis over time may provide information about the psychobiological state of the individual.

Discussion

Our approach to quantify HPPs demonstrates rapid graying transitions and their natural transitory reversal within individual human hair follicles at a higher frequency and with different kinetics than had previously been appreciated. The literature generally assumes pigment production in the HFPU to be a continuous process for the entire duration of an anagen cycle, but here we document a complete switch-on/off phenomena during a single anagen cycle. The proteomic features of hair graying directly implicate metabolic pathways that are both reversible in nature and sensitive to stress-related neuroendocrine factors. This result therefore provides a plausible biological basis for the rapid reversibility of graying and its association with psychological factors, and also supports the possibility that this process could be targeted pharmacologically. Melanogenesis is also known to both involve and respond to oxidative stress, a byproduct of mitochondrial metabolic processes[81] and driver of senescence[82]. Moreover, alterations in energy metabolism is a major contributor to other disease-related aging features[83], including lifespan regulation[84,85]. The upregulation of specific components related to mitochondrial energy metabolism in white hairs suggests that energy metabolism regulates not only hair growth as previously demonstrated[19,86,87] but also HS graying biology.

Although surprising, the reversal of hair graying is not an isolated case of “rejuvenation” in mammals. *In vivo*, exposing aged mice to young blood in parabiosis experiments[88,89] or diluting age-related factors in old animals[90] triggers the reversal of age-related molecular, structural and functional impairments. In human cells, quantitative biological age indicators such as telomere length[91] and DNA methylation[92] also exhibit temporary reversal in response to exercise and dietary interventions. Moreover, the reversibility of graying in aging human HFs demonstrated by our data is also consistent with the observed reversibility of human skin aging *in vivo* when aged human skin is xenotransplanted onto young nude mice[93]. Notably this skin “rejuvenation” is associated with a marked increase in the number of melanocytes in human epidermis[94], suggesting plasticity of the melanocyte compartment. Therefore, our HPP data and simulation model adds to a growing body of evidence demonstrating that human aging is not a linear, fixed biological process but may, at least in part, be halted or even temporarily reversed.

Our method to map the rapid (weeks to months) and natural reversibility of human hair graying may thus provide a powerful model to explore the malleability of human aging biology within time scales substantially smaller than the entire lifespan.

A surprising finding from both proteomics experiments is the bias towards *up*regulation rather than the loss of proteins in depigmented gray HS. As noted above, this may reflect the fact that hair graying is an actively regulated process within the HPFU, and that aging is not marked by a loss, but rather an increase in heterogeneity and biological complexity[5-8]. Relative to the youthful state, quiescent and senescent cells exhibit upregulation of various secreted factors[2], as well as elevated metabolic activities[95], rather than global downregulation of cellular activities. Moreover, similar to the macroscopic appearance of hair graying, age-related senescence naturally occurs among cells heterogeneously scattered within tissues[96], and the age-related accumulation of senescence-associated DNA methylation changes among cell populations also exhibit stochasticity[97]. Our data reveal that the conserved principle of an age-related increase in molecular and cellular heterogeneity is reflected not only at the tissue level (mixture of dark and white hairs) but also in the graying hair proteome. Further work is required to determine if stochastic molecular aging processes, in specific cell types within the HF, account for the macroscopic instability of HFs graying visible on the human scalp.

Finally, in relation to psychobiological processes, the spatio-temporal resolution of the HPP approach also provides investigators with an instructive new research tool that allows to link hair graying and reversal events with psychosocial exposures at an unprecedented level of resolution. Here we provided proof-of-concept evidence that biobehavioral factors are closely linked to human hair graying dynamics. Our optical digitization approach thus extends previous attempts to extract temporal information from human hairs[98] and illustrate the utility of HPP profiling as an instructive and sensitive psychobiology research model. Visualizing and retrospectively quantifying the association of life exposures and HPPs may help to understand the embedding of stress in aging biology at different stages of the lifespan.

References

1 Tobin, D. J. The cell biology of human hair follicle pigmentation. *Pigment Cell Melanoma Res* **24**, 75-88, doi:10.1111/j.1755-148X.2010.00803.x (2011).

2 van Deursen, J. M. The role of senescent cells in ageing. *Nature* **509**, 439-446, doi:10.1038/nature13193 (2014).

3 Omori, S. *et al.* Generation of a p16 Reporter Mouse and Its Use to Characterize and Target p16(high) Cells In Vivo. *Cell Metab*, doi:10.1016/j.cmet.2020.09.006 (2020).

4 Bernard, B. A. The human hair follicle, a bistable organ? *Experimental Dermatology* **21**, 401-403, doi:10.1111/j.1600-0625.2012.01457.x (2012).

5 LaRocca, T. J., Cavalier, A. N. & Wahl, D. Repetitive elements as a transcriptomic marker of aging: Evidence in multiple datasets and models. *Aging Cell* **19**, doi:10.1111/acel.13167 (2020).

6 Bahar, R. *et al.* Increased cell-to-cell variation in gene expression in ageing mouse heart. *Nature* **441**, 1011-1014, doi:10.1038/nature04844 (2006).

7 Enge, M. *et al.* Single-Cell Analysis of Human Pancreas Reveals Transcriptional Signatures of Aging and Somatic Mutation Patterns. *Cell* **171**, 321-330 e314, doi:10.1016/j.cell.2017.09.004 (2017).

8 Martinez-Jimenez, C. P. *et al.* Aging increases cell-to-cell transcriptional variability upon immune stimulation. *Science* **355**, 1433-1436, doi:10.1126/science.aah4115 (2017).

9 de Mochel, N. S. R. *et al.* Sentinel p16INK4a+ cells in the basement membrane form a reparative niche in the lung. *bioRxiv*, 2020.2006.2010.142893, doi:10.1101/2020.06.10.142893 (2020).

10 Akin Belli, A., Etgu, F., Ozbas Gok, S., Kara, B. & Dogan, G. Risk Factors for Premature Hair Graying in Young Turkish Adults. *Pediatr Dermatol* **33**, 438-442, doi:10.1111/pde.12881 (2016).

11 Panhard, S., Lozano, I. & Loussouarn, G. Greying of the human hair: a worldwide survey, revisiting the '50' rule of thumb. *Br J Dermatol* **167**, 865-873, doi:10.1111/j.1365-2133.2012.11095.x (2012).

12 Nishimura, E. K., Granter, S. R. & Fisher, D. E. Mechanisms of hair graying: incomplete melanocyte stem cell maintenance in the niche. *Science* **307**, 720-724, doi:10.1126/science.1099593 (2005).

13 Paus, R. A neuroendocrinological perspective on human hair follicle pigmentation. *Pigment Cell Melanoma Res* **24**, 89-106, doi:10.1111/j.1755-148X.2010.00808.x (2011).

14 Arck, P. C. *et al.* Towards a "free radical theory of graying": melanocyte apoptosis in the aging human hair follicle is an indicator of oxidative stress induced tissue damage. *FASEB J* **20**, 1567-1569, doi:10.1096/fj.05-4039fje (2006).

15 Trueb, R. M. & Tobin, D. J. *Aging Hair*. (Springer, 2010).

16 Tobin, D. J. Age-related hair pigment loss. *Curr Probl Dermatol* **47**, 128-138, doi:10.1159/000369413 (2015).

17 Nagl, W. Different growth rates of pigmented and white hair in the beard: differentiation vs. proliferation? *Br J Dermatol* **132**, 94-97, doi:10.1111/j.1365-2133.1995.tb08631.x (1995).

18 Van Neste, D. & Tobin, D. J. Hair cycle and hair pigmentation: dynamic interactions and changes associated with aging. *Micron* **35**, 193-200, doi:10.1016/j.micron.2003.11.006 (2004).

19 Flores, A. *et al.* Lactate dehydrogenase activity drives hair follicle stem cell activation. *Nat Cell Biol* **19**, 1017-1026, doi:10.1038/ncb3575 (2017).

20 Williams, R., Philpott, M. P. & Kealey, T. Metabolism of freshly isolated human hair follicles capable of hair elongation: a glutaminolytic, aerobic glycolytic tissue. *J Invest Dermatol* **100**, 834-840, doi:10.1111/1523-1747.ep12476744 (1993).

21 Zhang, Z., Gong, J., Sviderskaya, E. V., Wei, A. & Li, W. Mitochondrial NCKX5 regulates melanosomal biogenesis and pigment production. *J Cell Sci* **132**, doi:10.1242/jcs.232009 (2019).

22 Basrur, V. *et al.* Proteomic analysis of early melanosomes: identification of novel melanosomal proteins. *J Proteome Res* **2**, 69-79, doi:10.1021/pr025562r (2003).

23 Lemasters, J. J. *et al.* Compartmentation of Mitochondrial and Oxidative Metabolism in Growing Hair Follicles: A Ring of Fire. *The Journal of investigative dermatology* **137**, 1434-1444, doi:10.1016/j.jid.2017.02.983 (2017).

24 McBride, A. K. & Bergfeld, W. F. Mosaic hair color changes in alopecia areata. *Cleve Clin J Med* **57**, 354-356, doi:10.3949/ccjm.57.4.354 (1990).

25 Komagamine, T., Suzuki, K. & Hirata, K. Darkening of white hair following levodopa therapy in a patient with Parkinson's disease. *Mov Disord* **28**, 1643, doi:10.1002/mds.25696 (2013).

26 Reynolds, N. J., Crossley, J., Ferguson, I. & Peachey, R. D. Darkening of white hair in Parkinson's disease. *Clin Exp Dermatol* **14**, 317-318, doi:10.1111/j.1365-2230.1989.tb01992.x (1989).

27 Ricci, F., De Simone, C., Del Regno, L. & Peris, K. Drug-induced hair colour changes. *Eur J Dermatol* **26**, 531-536, doi:10.1684/ejd.2016.2844 (2016).

28 Sieve, B. F. Clinical Achromotrichia. *Science* **94**, 257-258, doi:10.1126/science.94.2437.257 (1941).

29 Yoon, K. H., Kim, D., Sohn, S. & Lee, W. S. Segmented heterochromia in scalp hair. *J Am Acad Dermatol* **49**, 1148-1150, doi:10.1016/s0190-9622(03)00471-7 (2003).

30 Kobayashi, E. *et al.* Reversible hair depigmentation in a Japanese female treated with pazopanib. *J Dermatol* **41**, 1021-1022, doi:10.1111/1346-8138.12654 (2014).

31 Kavak, A., Akcan, Y. & Korkmaz, U. Hair repigmentation in a hepatitis C patient treated with interferon and ribavirin. *Dermatology* **211**, 171-172, doi:10.1159/000086455 (2005).

32 Paus, R., Langan, E. A., Vidali, S., Ramot, Y. & Andersen, B. Neuroendocrinology of the hair follicle: principles and clinical perspectives. *Trends Mol Med* **20**, 559-570, doi:10.1016/j.molmed.2014.06.002 (2014).

33 Navarini, A. A. & Trueb, R. M. Reversal of canities. *Arch Dermatol* **146**, 103-104, doi:10.1001/archdermatol.2009.337 (2010).

34 Comaish, S. White scalp hairs turning black--an unusual reversal of the ageing process. *Br J Dermatol* **86**, 513-514, doi:10.1111/j.1365-2133.1972.tb16105.x (1972).

35 Tobin, D. J. & Cargnello, J. A. Partial reversal of canities in a 22-year-old normal Chinese male. *Arch Dermatol* **129**, 789-791 (1993).

36 Tobin, D. J. & Paus, R. Graying: gerontobiology of the hair follicle pigmentary unit. *Exp Gerontol* **36**, 29-54, doi:10.1016/s0531-5565(00)00210-2 (2001).

37 O'Sullivan, J. N., C.; Picard, M.; Chéret, J.; Bedogni, B.; Tobin, DJ.; Paus, R. The biology of human hair greying. *Biol Rev* (2020).

38 Puterman, E. *et al.* Lifespan adversity and later adulthood telomere length in the nationally representative US Health and Retirement Study. *Proc Natl Acad Sci U S A* **113**, E6335-E6342, doi:10.1073/pnas.1525602113 (2016).

39 Epel, E. S. *et al.* Accelerated telomere shortening in response to life stress. *Proc Natl Acad Sci U S A* **101**, 17312-17315, doi:0407162101 [pii] 10.1073/pnas.0407162101 (2004).

40 Zhang, B. *et al.* Hyperactivation of sympathetic nerves drives depletion of melanocyte stem cells. *Nature* **577**, 676-681, doi:10.1038/s41586-020-1935-3 (2020).

41 LeBeau, M. A., Montgomery, M. A. & Brewer, J. D. The role of variations in growth rate and sample collection on interpreting results of segmental analyses of hair. *Forensic Sci Int* **210**, 110-116, doi:10.1016/j.forsciint.2011.02.015 (2011).

42 Douglass, A. E. in *Climatic Cycles and Tree Growth* Vol. vol. II. (Carnegie Institute of Washington, 1928).

43 Paus, R. & Cotsarelis, G. The biology of hair follicles. *N Engl J Med* **341**, 491-497, doi:10.1056/NEJM199908123410706 (1999).

44 Slominski, A. *et al.* Hair follicle pigmentation. *J Invest Dermatol* **124**, 13-21, doi:10.1111/j.0022-202X.2004.23528.x (2005).

45 Cho, S. B., Zheng, Z., Kim, J. Y. & Oh, S. H. Segmented heterochromia in a single scalp hair. *Acta Derm Venereol* **94**, 609-610, doi:10.2340/00015555-1790 (2014).

46 Tobin, D. J. Aging of the hair follicle pigmentation system. *Int J Trichology* **1**, 83-93, doi:10.4103/0974-7753.58550 (2009).

47 Franklin, R. N. *et al.* Proteomic genotyping: Using mass spectrometry to infer SNP genotypes in pigmented and non-pigmented hair. *Forensic Sci Int* **310**, 110200, doi:10.1016/j.forsciint.2020.110200 (2020).

48 Van Neste, D. Thickness, medullation and growth rate of female scalp hair are subject to significant variation according to pigmentation and scalp location during ageing. *European Journal of Dermatology* **14**, 28-32 (2004).

49 Adav, S. S. *et al.* Studies on the Proteome of Human Hair - Identification of Histones and Deamidated Keratins. *Sci Rep* **8**, 1599, doi:10.1038/s41598-018-20041-9 (2018).

50 Calvo, S. E., Clauser, K. R. & Mootha, V. K. MitoCarta2.0: an updated inventory of mammalian mitochondrial proteins. *Nucleic Acids Res* **44**, D1251-1257, doi:10.1093/nar/gkv1003 (2016).

51 Singh, B., Schoeb, T. R., Bajpai, P., Slominski, A. & Singh, K. K. Reversing wrinkled skin and hair loss in mice by restoring mitochondrial function. *Cell Death Dis* **9**, 735, doi:10.1038/s41419-018-0765-9 (2018).

52 Vidali, S. *et al.* Hypothalamic-pituitary-thyroid axis hormones stimulate mitochondrial function and biogenesis in human hair follicles. *J Invest Dermatol* **134**, 33-42, doi:10.1038/jid.2013.286 (2014).

53 Kloepper, J. E. *et al.* Mitochondrial function in murine skin epithelium is crucial for hair follicle morphogenesis and epithelial-mesenchymal interactions. *J Invest Dermatol* **135**, 679-689, doi:10.1038/jid.2014.475 (2015).

54 Silengo, M. *et al.* Hair anomalies as a sign of mitochondrial disease. *Eur J Pediatr* **162**, 459-461, doi:10.1007/s00431-003-1228-5 (2003).

55 Singh, S. K. *et al.* E-cadherin mediates ultraviolet radiation- and calcium-induced melanin transfer in human skin cells. *Exp Dermatol* **26**, 1125-1133, doi:10.1111/exd.13395 (2017).

56 Wood, J. M. *et al.* Senile hair graying: H2O2-mediated oxidative stress affects human hair color by blunting methionine sulfoxide repair. *FASEB J* **23**, 2065-2075, doi:10.1096/fj.08-125435 (2009).

57 Hardman, J. A. *et al.* The peripheral clock regulates human pigmentation. *J Invest Dermatol* **135**, 1053-1064, doi:10.1038/jid.2014.442 (2015).

58 Tobin, D. J. & Kauser, S. Hair melanocytes as neuro-endocrine sensors--pigments for our imagination. *Mol Cell Endocrinol* **243**, 1-11, doi:10.1016/j.mce.2005.09.001 (2005).

59 Gaspar, E. *et al.* Thyrotropin-releasing hormone selectively stimulates human hair follicle pigmentation. *J Invest Dermatol* **131**, 2368-2377, doi:10.1038/jid.2011.221 (2011).

60 Nahm, M., Navarini, A. A. & Kelly, E. W. Canities subita: a reappraisal of evidence based on 196 case reports published in the medical literature. *Int J Trichology* **5**, 63-68, doi:10.4103/0974-7753.122959 (2013).

61 Han, L. K. M. *et al.* Accelerating research on biological aging and mental health: Current challenges and future directions. *Psychoneuroendocrinology* **106**, 293-311 (2019).

62 Picard, M. *et al.* A mitochondrial health index sensitive to mood and caregiving stress. *Biol Psychiatry* **84**, 9-17, doi:10.1016/j.biopsych.2018.01.012 (2018).

63 Picard, M. & McEwen, B. S. Psychological Stress and Mitochondria: A Systematic Review. *Psychosom Med* **80**, 141-153, doi:10.1097/PSY.0000000000000545 (2018).
64 Schlaepfer, I. R. & Joshi, M. CPT1A-mediated Fat Oxidation, Mechanisms, and Therapeutic Potential. *Endocrinology* **161**, doi:10.1210/endocr/bqz046 (2020).
65 Bekeova, C. *et al.* Multiple mitochondrial thioesterases have distinct tissue and substrate specificity and CoA regulation, suggesting unique functional roles. *J Biol Chem* **294**, 19034-19047, doi:10.1074/jbc.RA119.010901 (2019).
66 Okado-Matsumoto, A. & Fridovich, I. Subcellular distribution of superoxide dismutases (SOD) in rat liver: Cu,Zn-SOD in mitochondria. *J Biol Chem* **276**, 38388-38393, doi:10.1074/jbc.M105395200 (2001).
67 Hoffmann, L., Rust, M. B. & Culmsee, C. Actin(g) on mitochondria - a role for cofilin1 in neuronal cell death pathways. *Biol Chem* **400**, 1089-1097, doi:10.1515/hsz-2019-0120 (2019).
68 Rehklau, K. *et al.* Cofilin1-dependent actin dynamics control DRP1-mediated mitochondrial fission. *Cell Death Dis* **8**, e3063, doi:10.1038/cddis.2017.448 (2017).
69 Nie, H. *et al.* O-GlcNAcylation of PGK1 coordinates glycolysis and TCA cycle to promote tumor growth. *Nat Commun* **11**, 36, doi:10.1038/s41467-019-13601-8 (2020).
70 Sung, G. J. *et al.* Targeting CPT1A enhances metabolic therapy in human melanoma cells with the BRAF V600E mutation. *Int J Biochem Cell Biol* **81**, 76-81, doi:10.1016/j.biocel.2016.10.019 (2016).
71 Sumantran, V. N., Mishra, P. & Sudhakar, N. Microarray analysis of differentially expressed genes regulating lipid metabolism during melanoma progression. *Indian J Biochem Biophys* **52**, 125-131 (2015).
72 Oh, C. T. *et al.* Superoxide dismutase 1 inhibits alpha-melanocyte stimulating hormone and ultraviolet B-induced melanogenesis in murine skin. *Ann Dermatol* **26**, 681-687, doi:10.5021/ad.2014.26.6.681 (2014).
73 Bracalente, C. *et al.* Cofilin-1 levels and intracellular localization are associated with melanoma prognosis in a cohort of patients. *Oncotarget* **9**, 24097-24108, doi:10.18632/oncotarget.25303 (2018).
74 Morvan, D., Steyaert, J. M., Schwartz, L., Israel, M. & Demidem, A. Normal human melanocytes exposed to chronic insulin and glucose supplementation undergo oncogenic changes and methyl group metabolism cellular redistribution. *Am J Physiol Endocrinol Metab* **302**, E1407-1418, doi:10.1152/ajpendo.00594.2011 (2012).
75 Wiley, C. D. & Campisi, J. From Ancient Pathways to Aging Cells-Connecting Metabolism and Cellular Senescence. *Cell Metab* **23**, 1013-1021, doi:10.1016/j.cmet.2016.05.010 (2016).
76 Halloy, J., Bernard, B. A., Loussouarn, G. & Goldbeter, A. Modeling the dynamics of human hair cycles by a follicular automaton. *Proc Natl Acad Sci U S A* **97**, 8328-8333, doi:10.1073/pnas.97.15.8328 (2000).
77 Kinzina, E. D., Podolskiy, D. I., Dmitriev, S. E. & Gladyshev, V. N. Patterns of Aging Biomarkers, Mortality, and Damaging Mutations Illuminate the Beginning of Aging and Causes of Early-Life Mortality. *Cell Rep* **29**, 4276-4284 e4273, doi:10.1016/j.celrep.2019.11.091 (2019).
78 Patel, K. V. *et al.* Red cell distribution width and mortality in older adults: a meta-analysis. *J Gerontol A Biol Sci Med Sci* **65**, 258-265, doi:10.1093/gerona/glp163 (2010).
79 Stenn, K. S. & Paus, R. Controls of hair follicle cycling. *Physiol Rev* **81**, 449-494, doi:10.1152/physrev.2001.81.1.449 (2001).
80 Robbins, C. R. *The Chemical and Physical Behavior of Human Hair*. (Springer, 2012).
81 Balaban, R. S., Nemoto, S. & Finkel, T. Mitochondria, oxidants, and aging. *Cell* **120**, 483-495, doi:S0092-8674(05)00109-1 [pii] 10.1016/j.cell.2005.02.001 (2005).

82 Vizioli, M. G. *et al.* Mitochondria-to-nucleus retrograde signaling drives formation of cytoplasmic chromatin and inflammation in senescence. *Genes Dev* **34**, 428-445, doi:10.1101/gad.331272.119 (2020).
83 Kennedy, B. K. *et al.* Geroscience: linking aging to chronic disease. *Cell* **159**, 709-713, doi:10.1016/j.cell.2014.10.039 (2014).
84 Latorre-Pellicer, A. *et al.* Mitochondrial and nuclear DNA matching shapes metabolism and healthy ageing. *Nature* **535**, 561-565, doi:10.1038/nature18618 (2016).
85 Jang, J. Y., Blum, A., Liu, J. & Finkel, T. The role of mitochondria in aging. *J Clin Invest* **128**, 3662-3670, doi:10.1172/JCI120842 (2018).
86 Mancino, G. *et al.* The Thyroid Hormone Inactivator Enzyme, Type 3 Deiodinase, Is Essential for Coordination of Keratinocyte Growth and Differentiation. *Thyroid*, doi:10.1089/thy.2019.0557 (2020).
87 Ramot, Y. *et al.* Spermidine promotes human hair growth and is a novel modulator of human epithelial stem cell functions. *PLoS One* **6**, e22564, doi:10.1371/journal.pone.0022564 (2011).
88 Villeda, S. A. *et al.* Young blood reverses age-related impairments in cognitive function and synaptic plasticity in mice. *Nat Med* **20**, 659-663, doi:10.1038/nm.3569 (2014).
89 Rebo, J. *et al.* A single heterochronic blood exchange reveals rapid inhibition of multiple tissues by old blood. *Nat Commun* **7**, 13363, doi:10.1038/ncomms13363 (2016).
90 Mehdipour, M. *et al.* Rejuvenation of three germ layers tissues by exchanging old blood plasma with saline-albumin. *Aging (Albany NY)* **12**, 8790-8819, doi:10.18632/aging.103418 (2020).
91 Puterman, E. *et al.* Aerobic exercise lengthens telomeres and reduces stress in family caregivers: A randomized controlled trial - Curt Richter Award Paper 2018. *Psychoneuroendocrinology* **98**, 245-252, doi:10.1016/j.psyneuen.2018.08.002 (2018).
92 Fahy, G. M. *et al.* Reversal of epigenetic aging and immunosenescent trends in humans. *Aging Cell* **18**, e13028, doi:10.1111/acel.13028 (2019).
93 Gilhar, A., Pillar, T. & David, M. Aged versus young skin before and after transplantation onto nude mice. *Br J Dermatol* **124**, 168-171, doi:10.1111/j.1365-2133.1991.tb00427.x (1991).
94 Gilhar, A., Pillar, T., David, M. & Eidelman, S. Melanocytes and Langerhans cells in aged versus young skin before and after transplantation onto nude mice. *J Invest Dermatol* **96**, 210-214, doi:10.1111/1523-1747.ep12461330 (1991).
95 Lemons, J. M. *et al.* Quiescent fibroblasts exhibit high metabolic activity. *PLoS Biol* **8**, e1000514, doi:10.1371/journal.pbio.1000514 (2010).
96 Baker, D. J. *et al.* Naturally occurring p16(Ink4a)-positive cells shorten healthy lifespan. *Nature* **530**, 184-189, doi:10.1038/nature16932 (2016).
97 Franzen, J. *et al.* Senescence-associated DNA methylation is stochastically acquired in subpopulations of mesenchymal stem cells. *Aging Cell* **16**, 183-191, doi:10.1111/acel.12544 (2017).
98 Kalliokoski, O., Jellestad, F. K. & Murison, R. A systematic review of studies utilizing hair glucocorticoids as a measure of stress suggests the marker is more appropriate for quantifying short-term stressors. *Sci Rep* **9**, 11997, doi:10.1038/s41598-019-48517-2 (2019).
99 Picard, M., White, K. & Turnbull, D. M. Mitochondrial morphology, topology, and membrane interactions in skeletal muscle: a quantitative three-dimensional electron microscopy study. *Journal of applied physiology* **114**, 161-171, doi:10.1152/japplphysiol.01096.2012 (2013).
100 Goecker, Z. C. *et al.* Optimal processing for proteomic genotyping of single human hairs. *Forensic Sci Int Genet* **47**, 102314, doi:10.1016/j.fsigen.2020.102314 (2020).

101 Thompson, A. *et al.* Evaluation of the current knowledge limitations in breast cancer research: a gap analysis. *Breast Cancer Res* **10**, R26, doi:bcr1983 [pii] 10.1186/bcr1983 (2008).

102 Cox, J. *et al.* Andromeda: a peptide search engine integrated into the MaxQuant environment. *J Proteome Res* **10**, 1794-1805, doi:10.1021/pr101065j (2011).

103 Schaab, C., Geiger, T., Stoehr, G., Cox, J. & Mann, M. Analysis of high accuracy, quantitative proteomics data in the MaxQB database. *Mol Cell Proteomics* **11**, M111 014068, doi:10.1074/mcp.M111.014068 (2012).

104 Ge, S. X., Jung, D. & Yao, R. ShinyGO: a graphical enrichment tool for animals and plants. *Bioinformatics*, doi:10.1093/bioinformatics/btz931 (2019).

105 Szklarczyk, D. *et al.* STRING v11: protein-protein association networks with increased coverage, supporting functional discovery in genome-wide experimental datasets. *Nucleic Acids Res* **47**, D607-D613, doi:10.1093/nar/gky1131 (2019).

106 Gustafsson, C. M., Falkenberg, M. & Larsson, N. G. Maintenance and Expression of Mammalian Mitochondrial DNA. *Annu Rev Biochem* **85**, 133-160, doi:10.1146/annurev-biochem-060815-014402 (2016).

107 Kim, Y., Kim, H. D. & Kim, J. Cytoplasmic ribosomal protein S3 (rpS3) plays a pivotal role in mitochondrial DNA damage surveillance. *Biochim Biophys Acta* **1833**, 2943-2952, doi:10.1016/j.bbamcr.2013.07.015 (2013).

108 Lin, W. *et al.* The association of receptor of activated protein kinase C 1(RACK1) with infectious bursal disease virus viral protein VP5 and voltage-dependent anion channel 2 (VDAC2) inhibits apoptosis and enhances viral replication. *J Biol Chem* **290**, 8500-8510, doi:10.1074/jbc.M114.585687 (2015).

109 Belli, R. F. The structure of autobiographical memory and the event history calendar: potential improvements in the quality of retrospective reports in surveys. *Memory* **6**, 383-406, doi:10.1080/741942610 (1998).

110 van der Vaart, W. The time-line as a device to enhance recall in standardized research interviews: a split ballot study. *J Off Stat* **20**, 17 (2004).

111 Glasner, T. & van der Vaart, W. Applications of calendar instruments in social surveys: a review. *Qual Quant* **43**, 333-349, doi:10.1007/s11135-007-9129-8 (2009).

112 Sobell, L. C., Sobell, M. B., Leo, G. I. & Cancilla, A. Reliability of a timeline method: assessing normal drinkers' reports of recent drinking and a comparative evaluation across several populations. *Br J Addict* **83**, 393-402, doi:10.1111/j.1360-0443.1988.tb00485.x (1988).

113 Picard, M. *et al.* Mitochondrial dysfunction and lipid accumulation in the human diaphragm during mechanical ventilation. *American journal of respiratory and critical care medicine* **186**, 1140-1149, doi:10.1164/rccm.201206-0982OC (2012).

114 Fischer, H. *et al.* Essential role of the keratinocyte-specific endonuclease DNase1L2 in the removal of nuclear DNA from hair and nails. *J Invest Dermatol* **131**, 1208-1215, doi:10.1038/jid.2011.13 (2011).

115 R: A language and environment for statistical computing. (R Foundation for Statistical Computing, Vienna, Austria, 2010).

116 Chong, J., Wishart, D. S. & Xia, J. Using MetaboAnalyst 4.0 for Comprehensive and Integrative Metabolomics Data Analysis. *Curr Protoc Bioinformatics* **68**, e86, doi:10.1002/cpbi.86 (2019).

Methods

Participants

The study was approved by New York State Psychiatric Institute (NYSPI IRB Protocol #7748). All participants provided written informed consent. Dark, white, and bi-color hairs were collected from healthy participants self-identified as “having some gray hairs” or “two-colored hairs”. Exclusion criteria included the use of dye, bleaching, or other chemical treatments on hairs. In addition, participants with hairs shorter than approximately 4 cm were excluded. Participants were recruited via local advertisement and using a snowball recruitment strategy. Some participants were staff of NYSPI and Columbia University Irving Medical Center, but no patients participated in the study. Eligible participants were asked to provide all two-colored hairs present on their scalps or other body regions. A total of 14 individuals (7 females, 7 males), mean age 35 ± 13 (SD, range: 9-65), were recruited. Hairs were plucked, manually or with standard flat tip tweezers, from the scalp or other body regions and archived for future imaging or molecular analyses. Only plucked hairs with follicular tissue attached (excluding broken hairs) were used in analyses to enable the interpretation of the direction of pigmentation – transition if the HS tip is dark and the root white, reversal if the HS tip is white and the root dark. Where possible, participants with two-colored hairs also provided fully dark or white hairs for comparison.

While the participant age range doesn’t capture the typical range of an aged population, it provides an opportune window to examine the beginning of the aging process as it corresponds to the typical age of onset for graying or canities[46]. The hair follicles also manifest stochastic hair-to-hair heterogeneity similar to that seen between individual cells in aging organs[2,4]. For this reason, likely as a result of stochastic processes similar to those that drive cellular heterogeneity in gene expression, some HFs reach the end of their pigmented life even in relatively young individuals. Although the course and process of aging in middle age may differ from later aging, rare regimentation events are more likely to occur in the early stages of canities[18,37]. This is in accordance with our mathematical model (Figure 5) and with the isolated cases of repigmentation reported in the literature. Thus, to capture this phenomenon without additional confounds that could arise from systemic aging (comorbidities, systemic inflammation, or other), we focused our investigation on this particular age window. As our model predicts, this age window also increases the probability that hairs are near their graying threshold, and as such have the possibility to undergo observable reversal.

Hair imaging

Whole hairs were first photographed using a Panasonic DC-FZ80 Digital Camera against a white background, with the hair tip and follicle systematically oriented. To facilitate visualization of the images of whole hairs in the figures (photographic insets of whole hairs), the exposure, saturation, sharpness and light/dark tones of the photographs were enhanced. For microscopic imaging of hair follicles and HFPU, individual hair shafts and root-ends were imaged with an Olympus BX61 upright microscope equipped with a digitized stage (ProScan; Prior Scientific), a 2.5x/0.075 air (Zeiss, Germany), 10x/0.4 air (Zeiss, Germany) or 40x/1.3 oil (Olympus, MA) objectives, using DP71 camera (Olympus, MA) and MetaMorph software (Molecular Devices, CA) version 7.7.7.0. Images were scaled and analyzed in ImageJ (version 1.42q, NIH, http://rsb.info.nih.gov/ij). For microscopic imaging of hair shafts and videos of HPP transitions along the length of hair shafts, hairs were temporarily mounted with water on a glass slide (10x magnification, 15ms exposure, 24-bit, ISO 1600, 4080x3072 digitizer).

Digitization of hair pigmentation patterns

To generate high-resolution hair pigmentation patterns (HPPs), HSs were digitized as high-resolution 8-bit Grayscale images (3,200dpi, default adjustments, Epson Perfection V800 Photo Scanner), and the scanned images were processed using Image J (Fiji). To capture both the white and dark sections of each hair, hairs were immobilized onto a smooth surface by taping the plucked hair follicle (proximal to the epidermis), straightening the entire length as much as possible without placing too much force on the hair, and immobilizing the tip (distal to epidermis) with adhesive tape. HSs were dry and were checked for potential knots or twists caused by handling. Any dust was removed from the hair surface using a kimwipe before being placed on the scanner. Areas of each hair between the immobilized ends were used for analyses. To extract hair darkness at each point along the length, pixel luminosity at each position was estimated as the darkest value across a sliding one-dimensional pixels array perpendicular to the shaft axis, where the hair itself represented the darkest area, and HPP graphs were generated by plotting the intensity in arbitrary units (A.U.) by distance (cm). Intensity ranged from 0-255 A.U., with 0 being white and 255 being black. The data was then denoised using a 100-pixels rolling average, and the resulting HPP was imported into Prism 8 for visualization.

To compare intensity profiles across multiple hairs we transformed numerical intensity values by normalizing to the average intensity of each hair. A total of 100 randomly selected dark hairs were manually plucked from one female and one male individual, including 25 hairs per head region (left and right temporal, top, and crown). Digitized hairs for each individual were

graphed as a heatmap, grouped by head region. To examine the hypothesis that hairs exhibit regional variation in HPPs, the intensity of all 25 hairs per region were then averaged to create an 'average' hair from each region. A plot was then made for the four 'average hairs', one from each head region.

Electron microscopy

Dark and white scalp hairs were plucked from two healthy individuals: a 38-year-old African American male, a 33-year-old Caucasian male. The African American hairs were curly and black, while the Caucasian hairs were straight and auburn. Hairs were fixed in a 2% glutaraldehyde solution in 0.1 M cacodylate (TAAB Lab Equipment) buffer, pH 7.4 as described previously[99]. Briefly, plucked hair shafts were cut to 2-3 cm in length, immersed in fixative, and incubated at room temperature for 2 weeks. HS were then post-fixed and dehydrated in ethanol, cut into smaller segments of 0.5 cm, and embedded in longitudinal orientation in 100% resin. Orientation and section quality were confirmed with 1 µm-thick sections, and ultrathin sections of 70 nm were cut using a diamond knife on a Leica EM UC7 ultramicrotome. Sections mounted on Pioloform filmed copper grids prior to staining with 2% aqueous uranyl acetate and lead citrate (Leica). Ultrathin sections were examined on a Phillips CM 100 Compustage (FEI) transmission electron microscope and digital micrographs were captured by an AMT CCD camera.

Matched dark and white hairs from the donors were imaged, and three different segments along each hair were analyzed. All images used for analysis were captured at 7,500x magnification, with a pixel size of 0.00902 µm/pixel. Images were imported into ImageJ for analysis and all melanin granules contained within a given picture were manually traced (Intuos tablet). In each photograph, the intensity of the melanin granules, cortex, and background (outside the hair) were quantified. Cortex and melanin granule intensity were normalized by subtracting the background average intensity (measured from three different standard regions of interest – ROIs) to ensure comparability of various micrographs, hair segments, and between dark and white hairs. The intensity of the cortex was also quantified from eight different ROIs devoid of melanin granules.

To compute melanin granule size, we obtained the surface area of each manually traced granule. To compute melanin granule density per hair region, the total cortex area in each scaled micrograph was recorded and was divided by the total number of granules that were found in that image, yielding the number of granules/μm^2, which was then multiplied by 100.

Hair shaft proteomics

The protocol in both experiments 1 and 2 for hair digestion were adapted from a previous protocol establishing that SDS-based protein extraction methods results in higher protein yield than urea-based digestion[49]. This method was adapted with the addition of an initial mechanical homogenization step to extract proteins from minimal amounts of hair tissue (1-2 cm), which was necessary to analyze multiple hair segments along the same HS. After incubation, the hair was reduced with DTT and then alkylated with iodoacetamide (IAA), as per previous methods[100].

Experiment 1: For label-free quantitative proteomics, a 2-cm segment of plucked dark and white HS matched for distance relative to the follicle end was isolated from one female and one male participant. Each HS was washed independently in 20% methanol, ground and extracted in a glass homogenizer with SDS in Tris-buffered saline with 150-200ul of 4% protease inhibitor cocktail (Sigma P8340), precipitated with chloroform-methanol, redissolved in 8 M urea with ammonium bicarbonate, reduced, alkylated and digested with trypsin. For liquid chromatography and mass spectrometry two technical replicas (161 min chromatograms) were recorded for each sample. Separations were performed with an Ultimate 3000 RSLCNano (Thermo Scientific) on a 75 µm ID x 50 cm Acclaim PepMap reversed phase C18, 2 µm particle size column. Chromatographic flow rate was 300 nL/min with an acetonitrile/formic acid gradient. The liquid chromatograph was coupled to a Q Exactive HF mass spectrometer (Thermo Scientific) using data-dependent acquisition. Data were searched against a Swiss-Prot human protein database with Mascot v.2.5.1 (Matrix Science Ltd.). Semi-quantitative exponentially-modified protein abundance index (emPAI) was calculated by the Mascot software. A total of 744 proteins were detected. Proteins not detected in two or more samples from a total of 8 were not included for further analyses. Among the eligible proteins (n=323), the fold change in protein abundance was compared between white and dark hairs. The gene list (Supplemental Table S1) used for downstream analyses includes downregulated (<0.8-fold, n=23) and upregulated (>1.5-fold, n=67) proteins.

Experiment 2: 1 cm hair samples from each subject (n=17) were washed in 1 ml of 20% methanol while agitating at 1400 rpm for 20 mins at room temperature. The washed hair samples were homogenized using 150 µL of lysis buffer (4% SDS/0.1 M Tris/Protease inhibitor cocktail) in a glass homogenizer until no hair particles are visible. The lysates were incubated at 65^{o}C for 13 hours overnight at 1500 rpm. The next day, the samples were centrifuged at 20,000 x g for 10 mins to clear the lysate. Cleared lysates were reduced with 5 mM DTT at room temperature for 30 mins at 1000 rpm. Alkylation was carried out with 11 mM IAA at room temperature in the dark for 30 mins and quenched with 5 mM DTT for 15 mins at room

temperature. The proteins were precipitated using a chloroform-methanol method, and precipitated protein pellets were dissolved in 15 µL of resuspension buffer (4 M Urea/0.1 M Tris) and sonicated until entirely homogenized. Protein concentration was estimated using the BCA assay. 4 µg of total proteins from each sample was digested for 4 hours at 37°C with Lys-C protease at a 50:1 protein-to-protease ratio while shaking. Samples were then diluted with 100 mM Tris to bring down the urea concentration to the final 1.6 M and digested further with trypsin was then added at a 100:1 protein-to protease ratio, and the reaction was incubated overnight at 37°C. The next day, digestion was stopped by the addition of 1% TFA (final v/v) and centrifuged at 14,000 g for 10 min at room temperature. Cleared digested peptides were desalted on SDB-RP Stage-Tip and dried in a speed-vac. Peptides were dissolved in 3% acetonitrile/0.1% formic acid and 200 ng of peptides were injected on an Orbitrap Fusion Tribrid mass spectrometer (Thermo Scientific) coupled to an UltiMate 3000 UHPLC (Thermo Scientific). Peptides were separated on a 25 cm column (i.d. 75 µm, EASY-Spray, 2 µm, 100 Å) using a non-linear gradient of 5%-35% at a flow rate of 300 nl/min using a buffer B (0.1% (v/v) formic acid, 100% acetonitrile) for 90 min. After each gradient, the column was washed with 90 % buffer B for 5 min and re-equilibrated with 98% buffer A (0.1% formic acid, 100% HPLC-grade water) for 15 min. The full MS spectra were acquired in the Orbitrap from 400 to 1500 *m/z* at 120K with a 2 x 10^5 ion count target and a maximum injection time of 50 ms. The instrument was set to run in top speed mode with 3-second cycles for the survey and the MS/MS scans. After a survey scan, MS/MS was performed on the most abundant precursors, i.e., those exhibiting a charge state from 2 to 6 of greater than 5 x 10^3 intensity, by isolating them in the quadrupole at 1.6 Th. We used collision-induced dissociation (CID) with 35% collision energy and detected the resulting fragments with the rapid scan rate in the ion trap. The automatic gain control (AGC) target for MS/MS was set to 1 x 10^4, and the maximum injection time was limited to 35 ms. The dynamic exclusion was set to 30 s with a 10-ppm mass tolerance around the precursor and its isotopes. Monoisotopic precursor selection was enabled.

Raw mass spectrometric data were analyzed using the MaxQuant environment v.1.6.1.0[101] and Andromeda[102] for database searches at default settings with a few modifications. The default is used for first search tolerance and main search tolerance (20 ppm and 6 ppm, respectively). MaxQuant was set up to search with the reference human UniProtKB proteome database downloaded from UniProt. MaxQuant performed the search trypsin digestion with up to 2 missed cleavages. Peptide, site, and protein false discovery rates (FDR) were all set to 1% with a minimum of 1 peptide needed for identification; label-free quantitation (LFQ) was performed with a minimum ratio count of 1. To discriminate between relative and

absolute protein abundance, we also examined the intensity-based absolute quantification (iBAQ) values for each protein[103]. This allowed to discriminate between relative versus absolute upregulation of mitochondrial proteins. In particular, analysis of iBAQ data ensured that highly stoichiometric keratins and keratin-associated proteins were not downregulated in white hairs, and thus could not account for the observed upregulation of mitochondrial and other proteins. Search criteria included carbamidomethylation of cysteine as a fixed modification, oxidation of methionine, acetyl (protein N-terminus) and deamination for asparagine or glutamine (NQ) as variable modifications. A total of 438 proteins were detected. Proteins not detected in at least three samples from a total of 11 were not included in downstream analyses. Detected proteins not mapped to known genes are labeled as 'unknown'. From the eligible proteins (n=192), the fold change in protein abundance was compared between white and dark hairs. The gene list (Supplemental Table S2) used for downstream analyses includes downregulated (<0.8-fold, n=56) and upregulated (>1.5-fold, n=106) proteins. In sensitivity analyses, the data was re-analyzed with an alternate criterion of detection in at least 2 samples per color (≥2/6 dark, ≥2/5 white) and the data presented in **Supplemental Figure S10**.

For both Experiment 1 and 2, functional enrichment analysis was performed at an FDR threshold of 0.05 using Gene Ontology (GO) and Kyoto Encyclopedia of Genes and Genomes (KEGG) annotations in ShinyGO v.0.61 (http://bioinformatics.sdstate.edu/go/)[104]. Protein-protein interaction (PPI) networks were generated, analyzed for network metrics, and visualized in STRING v.11.0 (https://string-db.org/cgi/input.pl)[105]. Given the substantial representation of mitochondrial proteins among upregulated lists (67 of 323, 26.8% in Experiment 1; 21 of 106, 19.8% in white vs dark Experiment 2), we queried MitoCarta 2.0[50] and other sources, including GeneCards.org and database annotations to identify the following proteins as mitochondrial: HSP90B1, ASS1, MT-CO2[106], RPS3[107], RACK1[108], and ACOT7[65]. This search revealed enrichment of proteins related to energy metabolism and known to localize in mitochondria particularly among upregulated genes. We also queried the Human Lysosome Gene Database (http://lysosome.unipg.it/) to identify lysosomal proteins. In ShinyGO, networks of GO biological processes generated using a P-value cutoff for FDR of 0.01, and displaying top 20 most significant terms, with an edge cutoff of 0.2 were also examined to inform the functional categories that most accurately define both down- and upregulated proteins. PPI and GO biological processes networks are shown in Supplemental Figures S2-3.

Retrospective assessments of life events and stress

A subset of participants with noteworthy patterns of single-hair graying and reversal were asked to complete a retrospective stress assessment (**Supplemental Figure S6**), completed 1-4 months after hair collection in two individuals (one male, one female). The life event calendar (LEC) methodology increases the reliability and validity of recall in retrospective assessments[109]. The use of timeline results in higher accuracy and lowers underreporting as compared to traditional questionnaires[110]. The retrospective psychosocial stress assessment in the present study is an adaptation of LECs, more similar to timelines, which measures one behavioral construct – here "stress" – during a short reference period[111,112]. In our instrument, participants first position landmark events in time (in this case, the most stressful event or period, and the least stressful), and then link other events to these landmark events, a method referred to as sequencing[109]. Additionally, the visual calendar (see Figure S6) encourages top-down and parallel retrieval of memories[111], which also contributes to overall accuracy.

In the retrospective assessment, participants are first asked to identify the most stressful event or period over the last 12 months and to position it in time along the physical timeline, using their electronic calendar and objective dates, and assign it "10" on the graph. This first positioned event acts as a landmark event from which the other events can then be sequentially linked[109]. Participants then identified the least stressful event or period and assigned it "0" on the physical timeline, acting as another landmark event. Participants then indicated 2-6 additional particularly stressful events or periods, assigned them scores ranging from most stressful to least stressful (10 and 0, respectively), marked them on the timeline, and connected these events with a line that best illustrates their stress levels over the past year. The instrument not only asks the participant to mark their stress levels, but also to briefly name/describe each event, which can help with recall of the exact stressor and its intensity, and also allows participants to match up an event with an exact calendar date, enhancing the timing accuracy of events. Stress graphs were then digitized by aligning the retrospective assessment to a grid printed on transparency film, and the resulting digital values were plotted (Prism 8). To align stress profiles with HPP, digitized stress profiles were aligned with hairs from the same participant using dates of collection and assuming a hair growth rate of 1cm/month[41]. Each hair segment can then be mapped to specific weeks or month along the stress profile.

Hair shaft mtDNA quantification

Dark and white hairs (n=10 per person per color) were collected from the same two individuals whose hairs were analyzed by electron microscopy (African American male, Caucasian male). The follicle and proximal portion (2 cm segment) of the hair shaft were

sectioned and separately lysed in 200 µl of lysis buffer containing 500 mM Tris, 1% Tween 20, 20 µg/µl Proteinase K incubated for 10 hours at 55°C, followed by 10 min at 95°C as described previously[113]. Hair follicles were fully digested whereas the more robust proteinaceous hair shafts were only partially digested, such that the quantified mtDNA abundance is likely an underestimation of the total DNA amount per unit of hair shaft. In addition, nuclear DNA is rapidly degraded by endonucleases and virtually absent in the hair shaft[114]. We therefore focus our analysis of genomic material in the hair shaft to mtDNA.

The number of mtDNA copies per nucleated cell (mtDNA copy number, mtDNAcn) was measured by real-time quantitative polymerase chain reaction (qPCR) using a duplex Taqman reaction to amplify both mitochondrial (ND1) and nuclear DNA (B2M, single-copy gene) amplicons. The primer sequences are: (ND1-Fwd: GAGCGATGGTGAGAGCTAAGGT, ND1-Rev: CCCTAAAACCCGCCACATCT, Probe: HEX-CCATCACCCTCTACATCACCGCCC-3IABkFQ. B2M-Fwd: CCAGCAGAGAATGGAAAGTCAA, B2M-Rev: TCTCTCTCCATTCTTCAGTAAGTCAACT, Probe:FAMATGTGTCTGGGTTTCATCCATCCGACA-3IABkFQ) obtained from IDTdna.com. qPCR was performed on *QuantStudio™ 7 Flex Real-Time PCR System* (Applied Biosystems, Foster City, CA). Cycling conditions were as follows; 1 cycle of 50°C for 2 min, 95°C for 20 sec, followed by 40 cycles of 95°C for 1 sec, 60°C 20 sec.

For plucked hair follicles, all ND1 and B2M Cts were in the dynamic range of the assay and used to compute mtDNAcn from the ΔCt. All measures were performed in triplicates and the average Ct values taken for each sample. The mean C.V. for ND1 was 0.67% in both shafts and follicles, and for B2M 0.52% in follicles. mtDNAcn was calculated as $2^{\Delta Ct}$ (ND1 Ct - B2M Ct), and multiplied by 2 to take into account the diploid nature of the nuclear genome.

Mathematical modeling of graying dynamics across the lifespan

To simulate hair graying across the lifespan, a linear mixed effect model with random intercept and slopes to account for the stochastic process of hair graying was implemented in R[115]. This interactive implementation is available at https://timrain.shinyapps.io/hair. We first hypothesized a potential mechanism in which individual hairs are affected by a summation of effects from a random aging factor accumulating over time, random stress factor and random initial graying loading, thus creating variation between hairs within an individual. Once the hair has passed a prespecified threshold, the hair transitions to gray (**Figure 5B**). This model includes 17 parameters listed in **Supplemental Table S4**, each of which can be adjusted to

simulate various effects on individual hairs in relation to the aging process, including one or two stress exposure periods with customizable intensity and duration.

Scaling this model to hair populations with thousands of hairs, the simulation reports trajectories of graying for individual hairs, as well as a graph with the population distribution of white hairs (shown as frequency distributions) for a theoretical scalp. First, we simulated the average graying trajectory based on data indicating that the average age of onset for graying is age 35 and that white hairs reach a 40% population frequency at age 65[11]. This established a set of default parameters that yielded the graying trajectory shown in Figure 5C. We then simulated two hypothetical scenarios reflecting the total hair population for individuals who accumulate gray hairs at different rates, termed early and late grayers. These variable graying patterns were found to be generated by changing only one parameter, Sigma1, the standard deviation (across HFs) of the rate at which the aging factor increases over time.

Additionally, the model also simulated graying reversal, beginning with the parameters of the average grayer and then including also the stress parameters. To show the effect of stress on hair graying, we simulated two stressful periods starting at age 20 and then again at age 50, with equal intensity and duration. At age 20 the aging factor increases due to the stress but does not induce gray hair as the aging factor is still below the threshold (Figure 5E). On the other hand, at age 50 the same intensity and duration of the stressor will tend to induce additional graying as the aging factor for some hairs increases past the threshold, and then upon the end of the stressor, the aging factor could decrease past the threshold and thus the hair would undergo reversal (i.e., repigmentation) to its original color (Figure 5F).

An alternative model was considered to explore potential mechanisms for hair transitioning and reversal in response to stress. Specifically, we considered a mechanism in which the *rate* of accumulation in the aging factor increases during a period of stress (as opposed to our final model where stress causes a stepwise increase in aging factor) and then returns to the original rate following the end of the stressor. In this scenario, the threshold remains constant. This mechanism can be rejected because although it adequately simulates hair graying, once a hair has crossed above the threshold, if the stressor only affects the slope, it is not possible for a hair to return below threshold and undergo reversal (**Supplemental Figure S11**).

To simulate the graying process for a hypothetical person based on our hypothesized mechanism, we posited a linear mixed model for the ith ($i = 1, \ldots, n$) hair with two fixed effects (β_1 aging factor rate and β_2 stress sensitive rate) and three random effects (b_{i0} for graying

loading at age 0, b_{i1} for aging factor rate and b_{i2} for stress sensitive rate). To ensure positivity in age and accumulating stress, the model involves only the absolute value of each random effect.

$$GrayingLoading_{\{i,age\}} = |b_{i0}| + (|b_{i1}| + \beta_1)age + (|b_{i2}| + \beta_2)AccumulatingStress_{\{age\}} + e_{\{i,age\}}$$

Where $AccumulatingStress$ is defined as:

$$AccumulatingStress_{age} = \sum_{a=age-WindowWidth}^{age} stress_a$$

The three random effects follow a multivariate normal:

$$(b_{i0}, b_{i1}, b_{i2}) \sim N(0, G)$$

with covariance structure:

$$G = \begin{bmatrix} \sigma_0^2 & \rho_{01}\sigma_0\sigma_1 & \rho_{02}\sigma_0\sigma_2 \\ \rho_{01}\sigma_1\sigma_0 & \sigma_1^2 & \rho_{12}\sigma_1\sigma_2 \\ \rho_{02}\sigma_2\sigma_0 & \rho_{12}\sigma_2\sigma_1 & \sigma_2^2 \end{bmatrix}$$

All the correlations $\rho_{01}, \rho_{02}, \rho_{12}$ in the simulation are constrained to be positive. When the aging factor of hair i reaches a predefined threshold, the ith hair will turn white. The source code is available at https://github.com/junting-ren/hair_simulation.

Statistical analyses

An ordinary one-way ANOVA with Tukey's multiple comparison test was used to compare the number of melanin granules per μm^2, granule size, granule intensity, and relative intensity of the cortex in the dark and white hairs, and to compare the pigmentation intensity across head regions. To compare the rate of change in pigmentation per day between graying and reversal hairs, points of transitions visually estimated were used to derive a slope for each graying or reversal segment, which were compared using an unpaired t test.

A Mann-Whitney test was used to compare mtDNA levels in dark and white hair shafts and mtDNA copy number in dark and white hair follicles.

For univariate and multivariate analyses of proteomic signatures, protein abundance levels were processed in R using the Metaboanalyst 3.0 platform[116] as unpaired data. The data was mean-centered and log transformed prior to statistical analyses and missing (low abundance) values were imputed by half of the lowest value for the group (dark, white). Significance was established at an FDR level 0.05 and fold changes calculated using ANOVA. Partial least square discriminant analysis (PLS-DA) was used to extract meaningful features that

distinguish dark and white hairs and visualize groups of hairs or segments along the same hair. Two different strategies were used to generate protein lists subsequently queried for their functional significance: i) For dark vs white comparisons where the whole model is meaningful, the variable importance in projection (VIP) scores for each protein were extracted and used to select the top 40 most influential proteins (**Supplemental Figure S4C**); ii) For analyses of segments along the hair with graying followed by reversal, the factor loadings for each protein were extracted separately for components 1 and 2, and the top 20 positive and 20 negative proteins were selected for further analysis. Protein lists derived from both strategies were then used for functional enrichment analysis in ShinyGO and STRING as described above.

For the data displayed in Figure 3, we measured the strength of the temporal relationship between time series on the same scale (e.g., intensity measures of two hairs) by calculating the mean squared differences. The overall strength of temporal relationship among multiple time series is measured by the sum of all pairwise mean squared differences. To measure the strength of the temporal relationship between time series on different scales (specifically, intensity of color for a hair and rated level for stress levels) we calculated Pearson's correlation. To provide a reference distribution for comparison, we conducted 1000 random permutations of the data in each instance. For Figures 3A and 3B, each permutation involved simulating an equivalent number of hairs that transition (three hairs in 3A; two hairs in 3B). Each simulated hair includes a randomly selected transition placed at a random time point, with resampled noise before and after the transition. Two results are reported in each case. For the first, the library of transitions was taken from the transition segments of each observed hair, regardless of which direction (dark to white or white to dark) that transition was in. The probability of each direction of transition was determined by the overall rate of each transition direction from the observed data. The second reported result is based on a similar analysis, but the library of transitions included only the hairs that underwent the same directional change (dark-to-white in 3A; white-to-dark in 3B). The noise for uses of resampling was taken from hairs from the same subject after subtracting a smooth function, and resampling was done in segments of length-100 increments to maintain proper temporal correlation patterns. For Figure 3D, under the null hypothesis of no relationship between the hair intensity and stress pattern, each permutation involved choosing a random time point, splitting the stress pattern at that point and rejoining it by concatenating the two segments in the alternative order.

Acknowledgements

This work was supported by the Wharton Fund and NIH grants GM119793 and MH119336 (M.P.). The authors are grateful to Avsar Rana, David Sulzer, Marko Jovanonic, and to participants who donated hairs and time for this study.

Author contributions

A.R., S.R., R.K.S., P.P., G.S.: collected data. A.R., S.R., C.L., R.T.O., G.S., M.P.: analyzed data. J.R., R.T.O.: developed the simulation model with S.R., A.R., E.M.: performed imaging. M.P., R.P.: drafted manuscript. A.R. and D.J.T. revised manuscript. M.P., G.S.: designed study. All authors contributed to data interpretation and the final version of the manuscript.

Supplementary Information is available for this paper

The supplemental material includes 12 Figures (Figures S1-S12), 4 Tables (Tables S1-S4), and 1 Video (Video S1).

Data Availability

The datasets generated during and/or analyzed during the current study, including electron microscopy analysis (Figures 1, S1), HPPs (Figures 1-3, S5, S9), proteomic data (Figures 1, 3, 4, S2-4, S7, S10), and mtDNA data (Figure 4, S8) are available from the corresponding author upon request.

Code Availability

Source code for the hair simulation model is available on the App and on GitHub at https://github.com/junting-ren/hair_simulation

Correspondence and requests for materials should be addressed to Martin Picard, martin.picard@columbia.edu

Figure legends

Figure 1. Quantitative analysis of human hair pigmentation patterns, graying, and associated proteomic changes. (**A**) Diagram illustrating hair growth over time, method of hair collection, digitization, and hair pigmentation pattern (HPP) methodology. (**B**) Dark, white, and hairs undergoing natural age-related transitions from the younger dark state to the older white state at macroscopic and microscopic resolution. (**C**) Digitized HPPs for the hairs shown in (B). (**D**) Bright field microscopy images of hair follicles from plucked dark (top-panel) and white hair (bottom-panel) from the same Caucasian male individual illustrating the loss of pigmentation in the hair follicle pigmentary unit (HFPU). (**E**) Electron microscopic images of dark (*top*) and white (*bottom*) scalp hairs from a Caucasian male showing absent melanin granules in white hairs. (**F**) Quantification from dark (D) and white (W) hairs (n=3 segments from each) from a Caucasian (Cau.) male and African-American (AA) male of melanin granule abundance, (**G**) size and (**H**) darkness. (**I**) Overall electron density of the hair matrix (excluding granules) (N.S.). **J**) Volcano plot comparing dark and white hair proteomes and (**K**) heatmap of down- (<0.8-fold) and up-regulated (>1.5-fold) proteins that were detected in all samples (n=90) for experiment 1 (duplicates of dark/white hairs from 1 female, 1 male, n=8 samples). (**L**) Volcano plot and (**M**) heatmap for all proteins detected in $\geq$3 samples (n=192) from experiment 2 (dark and white hairs from 6 individuals, n=6 dark and 5 white hairs). Proteins annotated as mitochondrial (Mitocarta2.0) and lysosomal (The Human Lysosome Gene Database) are highlighted. Red dots to the right of heatmaps indicate mitochondrial proteins. *P<0.05, **P<0.01, ****P<0.0001 from one-way ANOVA, Tukey's multiple comparisons.

Figure 2 – Reversal of hair graying across ages and body regions. (**A-G**) Examples of HS graying and reversal including schematic of hair growth (*top left*), digitized HPP (*top right*), and light microscopy images (*bottom*) corresponding to numbered HS segments on the HPP plot. (**A**) Examples illustrating the reversal of graying along the length of scalp, (**B**) pubic, (**C**) and beard human HSs. (**D**) Example of segmental HS with double transitions, including temporary graying and (**E**) temporary reversal from an adult and a child, respectively. See Supplemental Figure S5 for additional examples and Video S1 for animation. (**F**) Time course diagram illustrating the progression of a single dark HS undergoing graying followed by reversal back to its original color, and (**G**) closely occurring events of graying and reversal occurring, producing HS with double transitions. (**H**) Average maximum and minimum pigmentation intensity among transitioning hairs from participants with two-colored hairs (n=11). Hairs with an average maximum intensity >180 A.U. are categorized as high intensity (black), 140-180 A.U. as intermediate intensity, and 100-140 A.U. as low intensity (pale color), indicating that these findings generalize across a range of pigmentation densities. (**I**) Rate of depigmentation per day in graying HS (n=23), measured from the slope on HPP graphs expressed as % of starting intensity loss per day (assuming growth rate of 1cm/month). (**J**) Comparison of the absolute rate of pigmentation change per day in graying (n=23) and reverted (n=34) HS. I and J are reported on a $\log_2$ scale to facilitate visualization.

Figure 3 – Synchronous graying and reversal behavior across multiple hairs and associations with psychosocial stress. (**A**) In a 35-year-old Caucasian female, multiple HS (n=3) undergoing graying simultaneously. (**B**) In a 37-year-old Caucasian female, two bi-color HS collected two months apart aligned based on a growth rate of 1 cm/month undergoing reversal nearly simultaneously. In A and B, simultaneously plucked dark and white hairs are plotted for reference. (**C**) In a 35-year old Caucasian male, multiple bi-color HS (n=5) undergoing reversal (top-panel) plotted against time-matched self-reported psychosocial stress levels (bottom-panel). (**D**) HS from a 30- year old Asian female with two months of self-reported profound perceived stress associated with temporary hair graying and reversal. Note the synchronicity between the increase in stress and rapid depigmentation (i.e., graying), followed by complete (103%) recovery of HS pigmentation (i.e., reversal of graying) upon alleviation of life stress. (**E**) Heatmap of protein abundance (n=301) across 6 segments: 2 dark prior to stress/graying, 2 white following graying, 2 dark segments after reversal. (**F**) Multivariate PLS-DA model of the 6 segments from the HS in E, highlighting the model's first and second principal components related to graying and reversal, respectively. Numbers 1 to 6 correspond to HS segments on D. (**G**) Factor loadings for Components 1 and 2 were used to extract the most significant proteins, subsequently analyzed for functional enrichment categories in KEGG and GO databases, and STRING protein networks. (**H**) Trajectories of protein abundance from the top Component 1 and (**I**) Component 2 features across the 6 segments; proteins with positive (*top*) and negative loadings (*bottom*) are shown separately.

Figure 4 – Meta-analysis of human hair proteomic findings comparing dark and white hairs. (**A**) Number of downregulated (<0.8-fold, blue) and upregulated (<1.5-fold) proteins across datasets, and unchanged proteins shown in grey. (**B**) Venn diagram illustrating the intersection of datasets. The number of overlapping proteins across datasets that are either consistently down- or upregulated, or proteins not regulated in the same direction, are shown for each area of overlap. (**C**) Individual protein abundance for consistently upregulated (n=5) and downregulated proteins (n=2) across experiments 1 and 2 shown are shown as box and whiskers plots, with bars extending from the 25^{th}-75^{th} percentiles, and whiskers from min to max values. Lines indicate the median and "+" signs indicate the mean. Fold difference values are the mean fold differences relative to dark hairs. (**D**) Mitochondrial DNA abundance in human HS of the same two donors as in Figures 1F-I (AA male, Cau male). (**E**) Summary of significantly enriched KEGG categories across datasets, for upregulated (*left*) and downregulated (*right*) proteins. (**F**) Correlation matrix (Spearman's r) of all detected proteins (n=192) in experiment 2, illustrating general human hair protein co-expression across dark and white pigmented states (dark, white). Four main clusters are highlighted and labeled by their top KEGG category. N.S. from Mann Whitney Test.

Figure 5 – Modeling of hair graying and reversal across the human lifespan and in response to temporary stress. (**A**) Schematic overview of the average graying process across the lifespan involving the gradual loss of pigmentation, or accumulation of white hairs, mostly in the second two-thirds of life. (**B**) Depiction of individual hairs (each line is a hair, i) from a linear mixed effects model with random

intercept and slopes predicting hair graying. The model assumes i) a constant increase in a putative aging factor and ii) a constant threshold above which hairs undergo depigmentation. All model parameters are listed in Supplemental Table S4. (**C**) Predicted hair population behavior (n=1,000 hairs) shown as a cumulative frequency distribution of white hairs from the individual trajectories in panel (B). (**D**) Frequency distributions of gray hairs for individuals with early (*left)*, average (*middle*), or late (*right*) hair graying phenotypes. The inset highlights a 2-year period during mid-life indicating gradual accumulation of white hairs, as well as the spontaneous repigmentation of a small fraction of white hairs (decrease in % white hairs), consistent with real-world data. **(E**) Single hair-level and (**F**) hair population-level results from the addition of two acute stress periods (each one year in duration, occurring at ages 20 and 50). The optimized model accounts for stress-induced graying in hairs whose aging factor is close to the depigmentation threshold, but not for young hairs or those far away from the threshold. Similarly, the removal of the stressor causes repigmentation of hairs when the aging factor returns below the threshold.

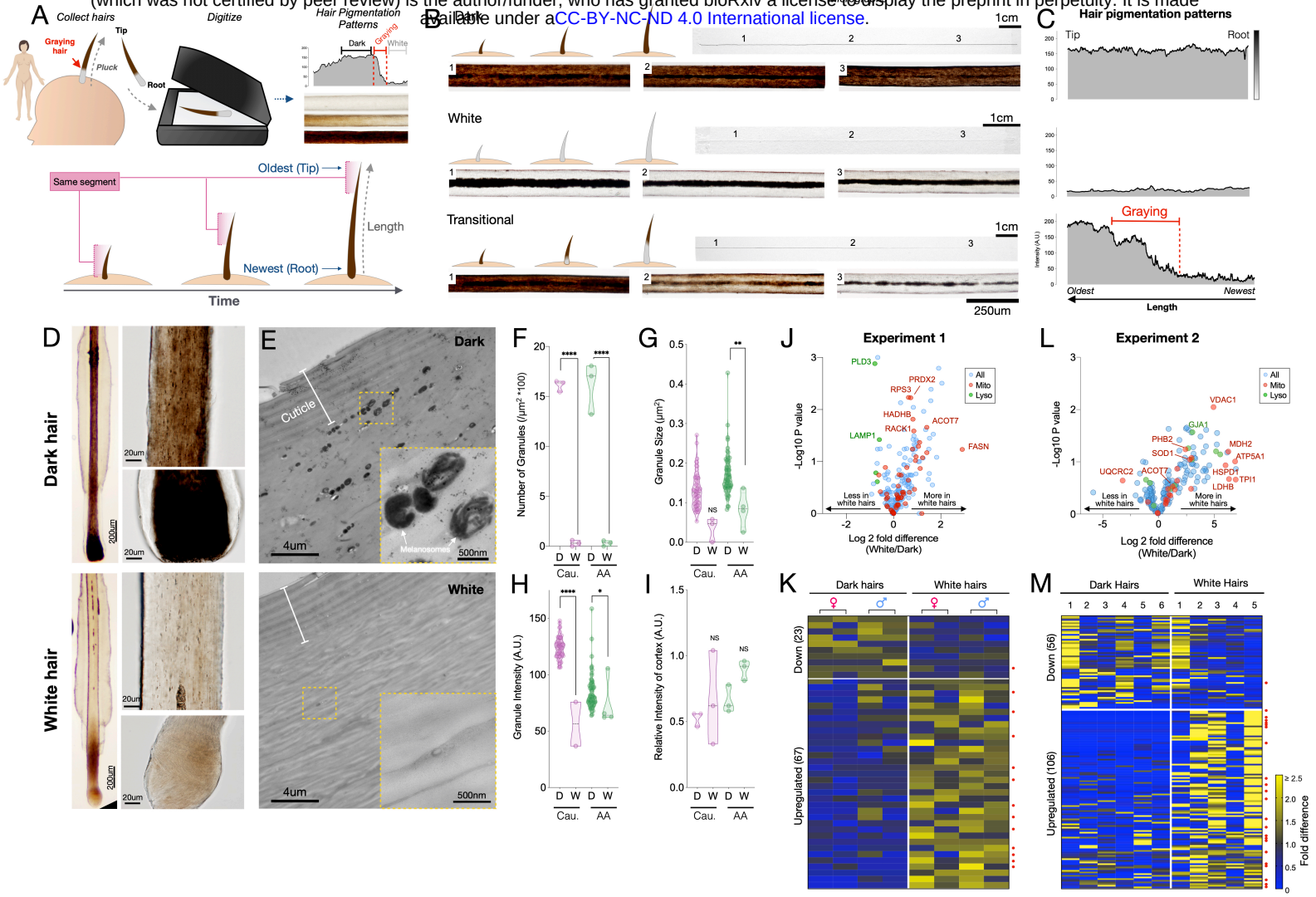

Figure 1. Quantitative analysis of human hair pigmentation patterns, graying, and associated proteomic changes. (**A**) Diagram illustrating hair growth over time, method of hair collection, digitization, and hair pigmentation pattern (HPP) methodology. (**B**) Dark, white, and hairs undergoing natural age-related transitions from the younger dark state to the older white state at macroscopic and microscopic resolution. (**C**) Digitized HPPs for the hairs shown in (B). (**D**) Bright field microscopy images of hair follicles from plucked dark (top-panel) and white hair (bottom-panel) from the same Caucasian male individual illustrating the loss of pigmentation in the hair follicle pigmentary unit (HFPU). (**E**) Electron microscopic images of dark (*top*) and white (*bottom*) scalp hairs from a Caucasian male showing absent melanin granules in white hairs. (**F**) Quantification from dark (D) and white (W) hairs (n=3 segments from each) from a Caucasian (Cau.) male and African-American (AA) male of melanin granule abundance, (**G**) size and (**H**) darkness. (**I**) Overall electron density of the hair matrix (excluding granules) (N.S.). **J**) Volcano plot comparing dark and white hair proteomes and (**K**) heatmap of down- (<0.8-fold) and up-regulated (>1.5-fold) proteins that were detected in all samples (n=90) for experiment 1 (duplicates of dark/white hairs from 1 female, 1 male, n=8 samples). (**L**) Volcano plot and (**M**) heatmap for all proteins detected in ≥3 samples (n=192) from experiment 2 (dark and white hairs from 6 individuals, n=6 dark and 5 white hairs). Proteins annotated as mitochondrial (Mitocarta2.0) and lysosomal (The Human Lysosome Gene Database) are highlighted. Red dots to the right of heatmaps indicate mitochondrial proteins. *P<0.05, **P<0.01, ****P<0.0001 from one-way ANOVA, Tukey's multiple comparisons.

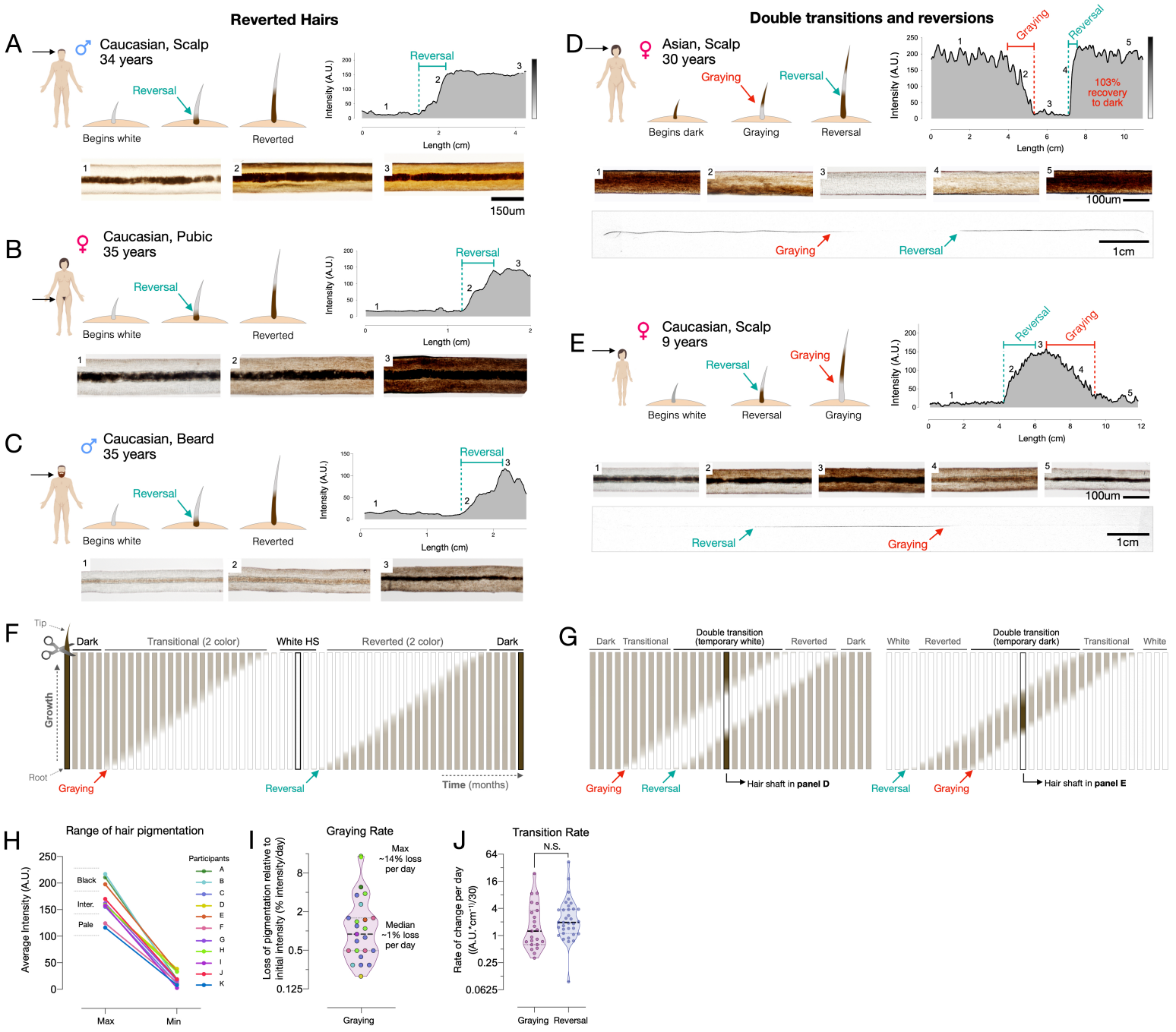

Figure 2 – Reversal of hair graying across ages and body regions. (**A-G**) Examples of HS graying and reversal including schematic of hair growth (*top left*), digitized HPP (*top right*), and light microscopy images (*bottom*) corresponding to numbered HS segments on the HPP plot. (**A**) Examples illustrating the reversal of graying along the length of scalp, (**B**) pubic, (**C**) and beard human HSs. (**D**) Example of segmental HS with double transitions, including temporary graying and (**E**) temporary reversal from an adult and a child, respectively. See Supplemental Figure S5 for additional examples and Video S1 for animation. (**F**) Time course diagram illustrating the progression of a single dark HS undergoing graying followed by reversal back to its original color, and (**G**) closely occurring events of graying and reversal occurring, producing HS with double transitions. (**H**) Average maximum and minimum pigmentation intensity among transitioning hairs from participants with two-colored hairs (n=11). Hairs with an average maximum intensity >180 A.U. are categorized as high intensity (black), 140-180 A.U. as intermediate intensity, and 100-140 A.U. as low intensity (pale color), indicating that these findings generalize across a range of pigmentation densities. (**I**) Rate of depigmentation per day in graying HS (n=23), measured from the slope on HPP graphs expressed as % of starting intensity loss per day (assuming growth rate of 1cm/month). (**J**) Comparison of the absolute rate of pigmentation change per day in graying (n=23) and reverted (n=34) HS. I and J are reported on a $\log_2$ scale to facilitate visualization.

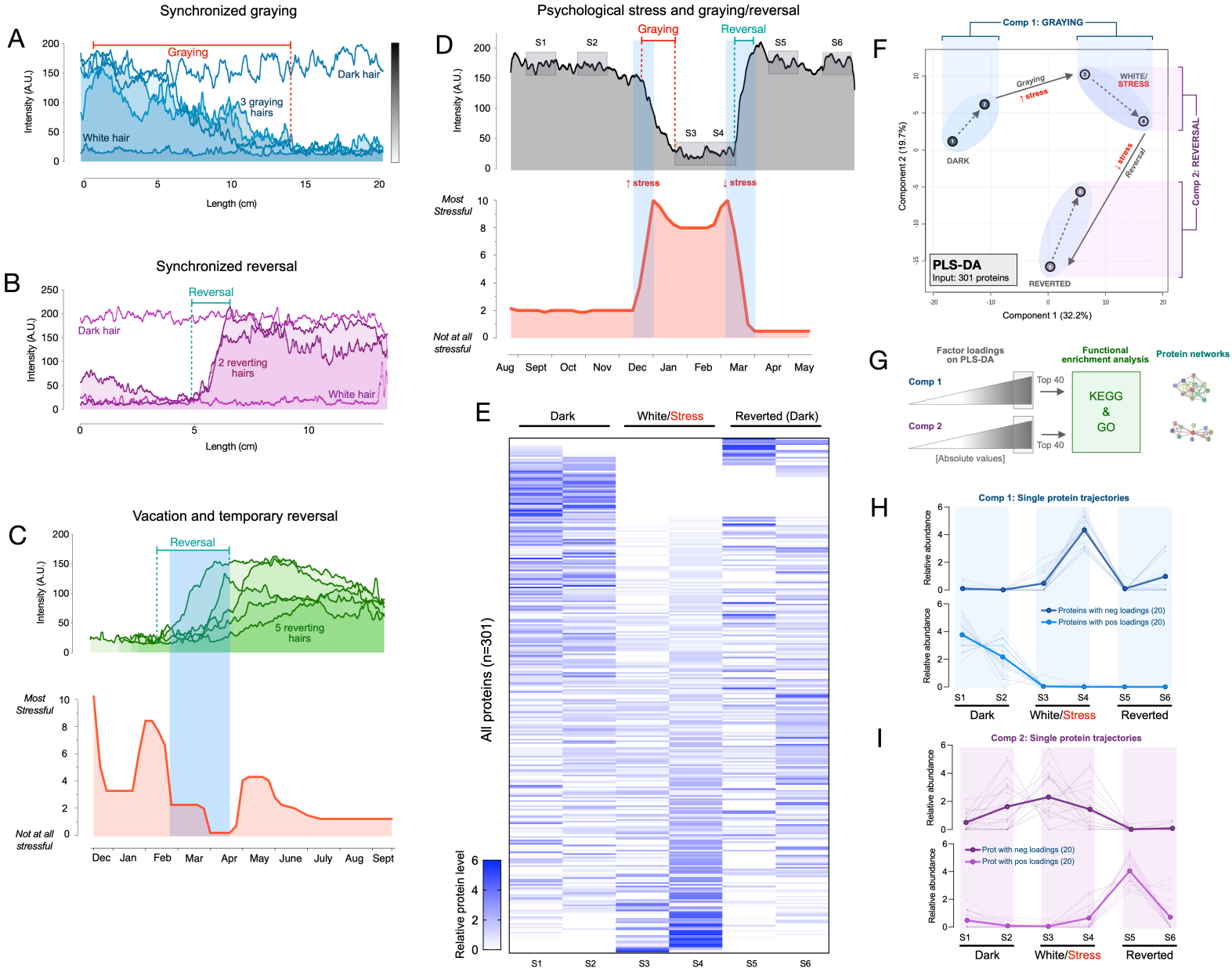

Figure 3 – Synchronous graying and reversal behavior across multiple hairs and associations with psychosocial stress. (**A**) In a 35-year old Caucasian female, multiple HS (n=3) undergoing graying simultaneously. (**B**) In a 37-year old Caucasian female, two bi-color HS collected two months apart aligned based on a growth rate of 1cm/month undergoing reversal nearly simultaneously. In A and B, simultaneously plucked dark and white hairs are plotted for reference. (**C**) In a 35-year old Caucasian male, multiple bi-color HS (n=5) undergoing reversal (top-panel) plotted against time-matched self-reported psychosocial stress levels (bottom-panel). (**D**) HS from a 30- year old Asian female with two months of self-reported profound perceived stress associated with temporary hair graying and reversal. Note the synchronicity between the increase in stress and rapid depigmentation (i.e., graying), followed by complete (103%) recovery of HS pigmentation (i.e., reversal of graying) upon alleviation of life stress. (**E**) Heatmap of protein abundance (n=301) across 6 segments: 2 dark prior to stress/graying, 2 white following graying, 2 dark segments after reversal. (**F**) Multivariate PLS-DA model of the 6 segments from the HS in E, highlighting the model's first and second principal components related to graying and reversal, respectively. Numbers 1 to 6 correspond to HS segments on D. (**G**) Factor loadings for Components 1 and 2 were used to extract the most significant proteins, subsequently analyzed for functional enrichment categories in KEGG and GO databases, and STRING protein networks. (**H**) Trajectories of protein abundance from the top Component 1 and (**I**) Component 2 features across the 6 segments; proteins with positive (*top*) and negative loadings (*bottom*) are shown separately.

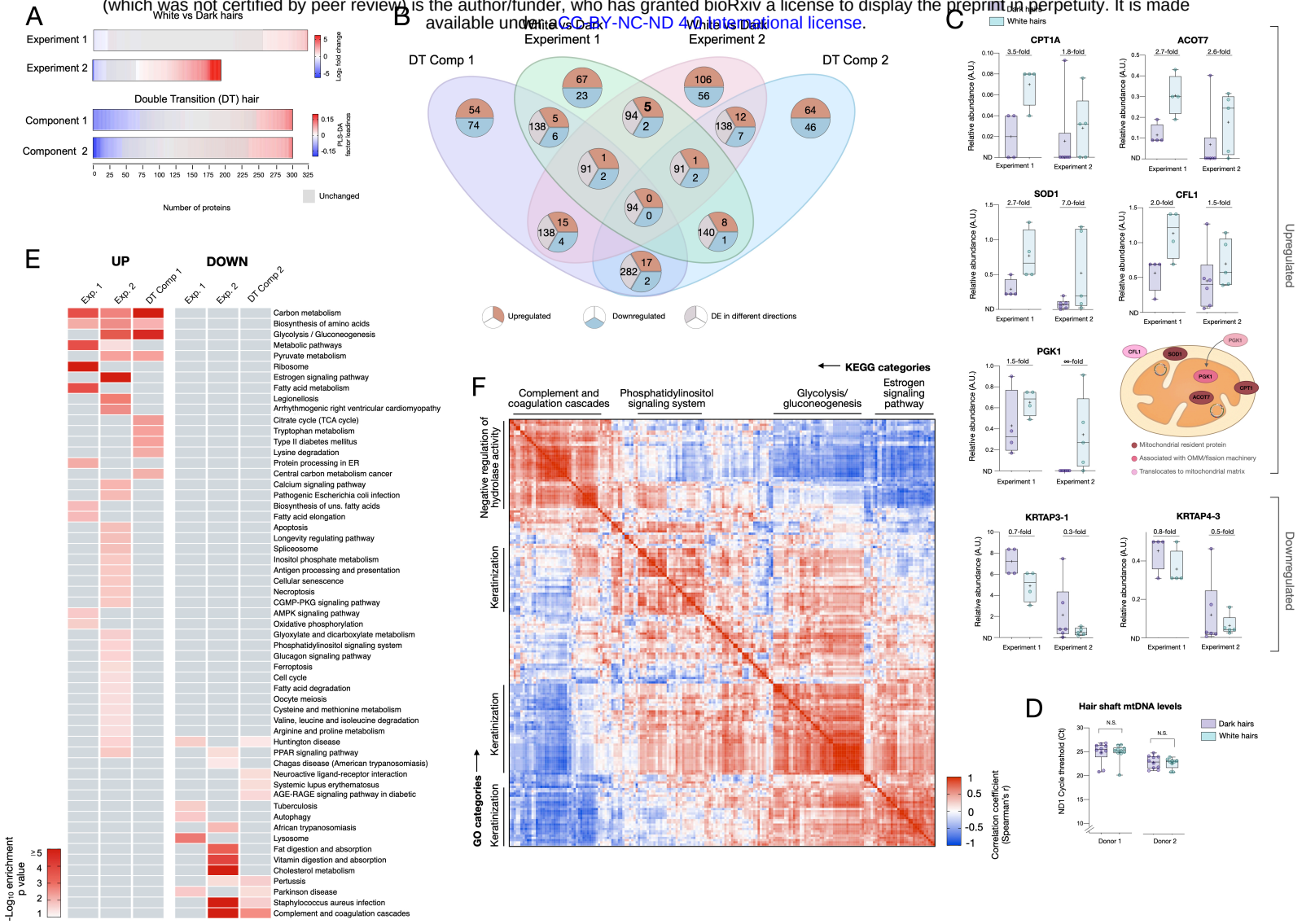

Figure 4 – Meta-analysis of human hair proteomic findings comparing dark and white hairs. (**A**) Number of downregulated (<0.8-fold, blue) and upregulated (<1.5-fold) proteins across datasets, and unchanged proteins shown in grey. (**B**) Venn diagram illustrating the intersection of datasets. The number of overlapping proteins across datasets that are either consistently down- or upregulated, or proteins not regulated in the same direction, are shown for each area of overlap. (**C**) Individual protein abundance for consistently upregulated (n=5) and downregulated proteins (n=2) across experiments 1 and 2 shown are shown as box and whiskers plots, with bars extending from the 25th-75th percentiles, and whiskers from min to max values. Lines indicate the median and "+" signs indicate the mean. Fold difference values are the mean fold differences relative to dark hairs. (**D**) Mitochondrial DNA abundance in human HS of the same two donors as in Figures 1F-I (AA male, Cau male). (**E**) Summary of significantly enriched KEGG categories across datasets, for upregulated (*left*) and downregulated (*right*) proteins. (**F**) Correlation matrix (Spearman's r) of all detected proteins (n=192) in experiment 2, illustrating general human hair protein co-expression across dark and white pigmented states (dark, white). Four main clusters are highlighted and labeled by their top KEGG category. N.S. from Mann Whitney Test.

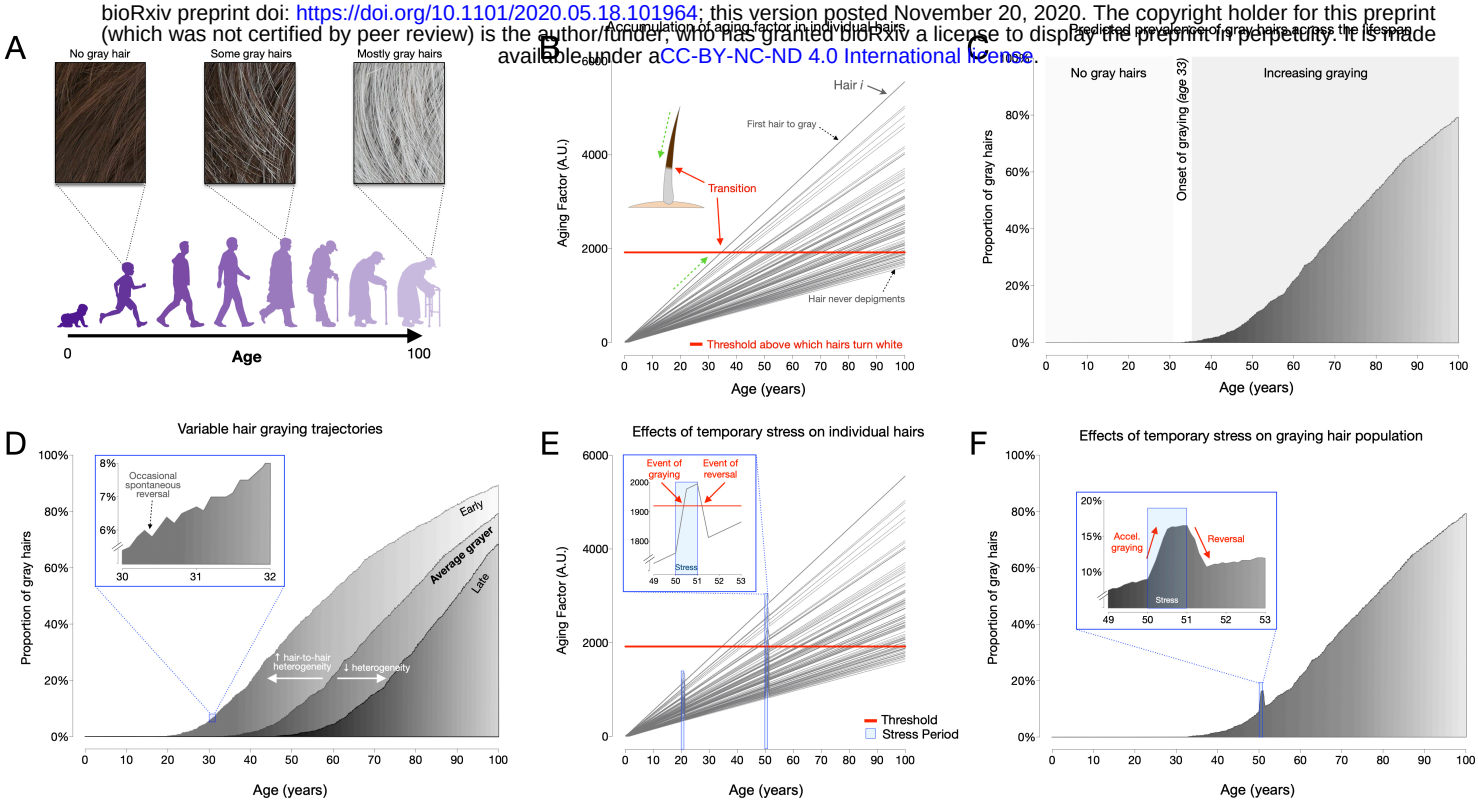

Figure 5 – Modeling of hair graying and reversal across the human lifespan and in response to temporary stress. (**A**) Schematic overview of the average graying process across the lifespan involving the gradual loss of pigmentation, or accumulation of white hairs, mostly in the second two-thirds of life. (**B**) Depiction of individual hairs (each line is a hair, i) from a linear mixed effects model with random intercept and slopes predicting hair graying. The model assumes i) a constant increase in a putative aging factor and ii) a constant threshold above which hairs undergo depigmentation. All model parameters are listed in Supplemental Table S4. (**C**) Predicted hair population behavior (n=1,000 hairs) shown as a cumulative frequency distribution of white hairs from the individual trajectories in panel (B). (**D**) Frequency distributions of gray hairs for individuals with early (*left)*, average (*middle*), or late (*right*) hair graying phenotypes. The inset highlights a 2-year period during mid-life indicating gradual accumulation of white hairs, as well as the spontaneous repigmentation of a small fraction of white hairs (decrease in % white hairs), consistent with real-world data. **(E**) Single hair-level and (**F**) hair population-level results from the addition of two acute stress periods (each one year in duration, occurring at ages 20 and 50). The optimized model accounts for stress-induced graying in hairs whose aging factor is close to the depigmentation threshold, but not for young hairs or those far away from the threshold. Similarly, the removal of the stressor causes repigmentation of hairs when the aging factor returns below the threshold.